A Review on Heterogeneous Nanostructures: A Strategy for Superior Mechanical Properties in Metals

Yan Ma [1,2,†] [ID], **Muxin Yang [1,†], Fuping Yuan [1,2,*] and Xiaolei Wu [1,2]**

1   State Key Laboratory of Nonlinear Mechanics, Institute of Mechanics, Chinese Academy of Sciences, No. 15, North 4th Ring, West Road, Beijing 100190, China; mayan@imech.ac.cn (Y.M.); mxyang@lnm.imech.ac.cn (M.Y.); xlwu@imech.ac.cn (X.W.)
2   School of Engineering Science, University of Chinese Academy of Sciences, No. 19(A) Yuquan Road, Shijingshan District, Beijing 100049, China
*   Correspondence: fpyuan@lnm.imech.ac.cn; Tel.: +86-10-8254-4409; Fax: +86-10-8254-3977
†   Y.M. and M.Y. contributed equally to this work.

check for updates

Abstract: Generally, strength and ductility are mutually exclusive in homogeneous metals. Nanostructured metals can have much higher strength when compared to their coarse-grained counterparts, while simple microstructure refinement to nanoscale generally results in poor strain hardening and limited ductility. In recent years, heterogeneous nanostructures in metals have been proven to be a new strategy to achieve unprecedented mechanical properties that are not accessible to their homogeneous counterparts. Here, we review recent advances in overcoming this strength–ductility trade-off by the designs of several heterogeneous nanostructures in metals: heterogeneous grain/lamellar/phase structures, gradient structure, nanotwinned structure and structure with nanoprecipitates. These structural heterogeneities can induce stress/strain partitioning between domains with dramatically different strengths, strain gradients and geometrically necessary dislocations near domain interfaces, and back-stress strengthening/hardening for high strength and large ductility. This review also provides the guideline for optimizing the mechanical properties in heterogeneous nanostructures by highlighting future challenges and opportunities.

Keywords: strength; ductility; heterogeneous nanostructures; back-stress hardening; strain gradient

1. Introduction

High strength in metals is always favorable in industry, while the elevation in strength is usually accompanied with the drastic loss in ductility [1–6]. High strength in metals can be achieved by grain refinement or cold working [1,7–10]. For the last several decades, severe plastic deformation has been extensively utilized to produce nanocrystalline (NC) or ultrafine-grained (UFG) metals with ultra-high strength [1,7–9], while the low strain hardening and the resultant limited ductility restrict their practical applications [2–5]. Thus, the main challenge is to design novel microstructures to restore an acceptable ductility in the high-strength metals and evade the strength–ductility trade-off.

Metals with both high strength and large ductility are always desired for the structural applications, and such demands have been realized in the last decade by the novel strategy: tailoring the microstructures at nanoscale, i.e., the design of heterogeneous nanostructures [2,3]. These heterogeneous nanostructures include heterogeneous grain/lamellar/phase structures [11–33], gradient structure [34–65], nanotwins [66–115], and nanoprecipitates [116–120]. One common feature in these heterogeneous nanostructures is that there always exist various domains with dramatically different strengths, although the geometrical patterns and the structural sizes of the domains might vary widely [3,14–17]. The inhomogeneous plastic deformation in different domains would cause

stress/strain partitioning and strain gradients at the domain interfaces [3,14–17]. And the strain gradients should produce geometrically necessary dislocations (GNDs) and extra-hardening for better performance in mechanical properties [11–30].

In this regard, we will present a review in recent advances for heterogeneous nanostructures, and the addressed points are focusing on mechanical properties, microstructure characterization, and deformation physics. In this review, experimental work, numerical simulations and theoretical analysis are all discussed.

2. Heterogeneous Grain/Lamella/Phase Structures

Heterogeneous grain/lamella/phase structures, either with or without dual/multiple constituent phases [17–22] and precipitates [23,24] have been regarded as a new class of ideal candidates for structural applications due to their high strength and excellent ductility [2,3]. In this type of materials, the interplays between different adjoining microdomains with different grain sizes, phase constitutes, and/or dislocation substructures are crucial to understand the mechanical behaviors and guide the designing of ultra-strong materials with good tensile ductility [2,3,11,12,15–29].

2.1. Hetero-Interfaces and Deformation Mechanisms

Hetero-interfaces in heterogeneous grain/lamella/phase structures are the domain boundaries created during fabrication and developed with the applied straining, and such interfaces bear striking similarities to the conventional grain boundaries (GBs), albeit obvious differences also exist between them [14,18]. In homogeneous materials, the flow stresses exerted on moveable dislocations due to the presence of GBs generally are short-ranged, whereas in heterogeneous grain/lamella/phase structures the extra flow stresses, exerted on the hetero-interfaces due to the directional pile-ups of GNDs, usually are long-ranged [3,13,121]. As a result, the GND pile-ups nucleated by inhomogeneous plastic flow also give rise to an additional inhomogeneous stress locally at the hetero-interfaces because the creation of the GND pile-ups against the hetero-interfaces hinders the successive sliding of mobile dislocations [3,14]. More importantly, the hetero-interfaces are mechanical incompatibility interfaces, which can accommodate inhomogeneous plastic deformation and release the stress concentration [28,122,123]. The hetero-interface is a kind of strain constraint interface that displays a dynamic existence between various adjacent hard/soft microdomains during loading [14]. The main functions of the hetero-interface include: i) accommodating local plastic strains; ii) providing extra strain hardening and additional strengthening effects [13,15,16]. It is well-known that the hetero-interface is the main factor governing the strengthening and strain-hardening behaviors of heterogeneous grain/lamella/phase structures. On one hand, the hard microdomains do not need to bear large plastic strain during deformation, while provide ultra-high strength to the whole sample due to the dynamically strain partitioning and the load transferring mechanisms [122–127]. On the other hand, the plastic straining of the soft microdomains occurs under the multiaxial stress constraints of the surrounding hard microdomains, thus their own strain hardening and strengthening can be greatly enhanced [16,18,53], resulting in better strength and ductility for the whole sample [13,16–19].

In fact, the superior mechanical properties of heterogeneous grain/lamella/phase structures can be attributed to the synergistic strengthening and strain hardening due to the mechanical incompatibility at the hetero-interfaces between adjacent soft/hard domains during plastic deformation [16,25]. Upon tensile loading, both the soft and hard domains are elastically deformed firstly, and after that, the soft domains yield first with increasing applied strain while the hard domains still deform elastically, which can create a strain gradient accommodated by GND pile-up at the hetero-interfaces [121,128]. The pile-up of GNDs in turn produces long-range back-stress strengthening to enhance global yield stress [13,16,121]. Since the back stress at the hetero-interface is high and is subsequently relieved to a certain extent due to the plastic deformation of a portion of hard domains, a macroscopic flow-stress dip or a transient hardening phenomenon may occur in the macroscopic stress–strain curves soon after

an overall yielding, which depends on the competition between the stress relaxation of hard domains and the hardening of soft domains [28,123,129–131].

2.2. Heterogeneous Grain Structures

As one of the most important microstructural parameters, the grain size plays a crucial role in controlling the yield strengths and strain-hardening behaviors in various metallic materials [1,4–10]. The domains in heterogeneous grain structure (HGS), containing grains with different sizes varying from nanometers to micrometers [14,17,18], and hence display dramatic strength difference from one domain to another according to the well-known Hall–Petch relationship.

According to the Considère criterion, tensile uniform elongation of high-strength metals can be effectively improved if plastic strain instability is suppressed [132]. One of the most effective methods for delocalizing plastic instability and enhancing strain-hardening rate is to fabricate HGS, which are composed of both nanograins (NGs) and coarse grains (CGs) [17]. Such materials with HGS have two and even more peaks in their grain size distributions which span widely through several orders of magnitude in general [17,18,133–135]. Accordingly, excellent synergy of high strength and good ductility has been observed in the resultant materials with HGS, due to their extraordinary strain-hardening capacities [14,17,18]. For example, the bi- and multi-modal microstructures were reported to have both high tensile yield strength and large uniform elongation in copper by simultaneously improving the dislocation accumulation capability and brittle-crack initiation resistance [18,133,134]. Although the deformation mechanisms of these approaches are still not fully understood, it can be generally inferred that the existence of the constrained soft CGs suppresses strain localization and enables extra strain-hardening, prolonging uniform elongation at high flow stresses, while the NGs bear load transfer and provide high strength [16,17,124,126]. The key factor in materials with HGS is that the plastic deformation is non-homogenous and the local deformation incompatibility can promote the macroscopic plastic strain in a more effective manner.

Since back stress hardening plays an important role during the plastic deformation of materials with HGS, the origin and the definition of back stress should be discussed first. The term "back stress" was first used in Fisher's research on the strengthening behaviors in a precipitation hardening alloy [136]. The back stress was referred as a reverse average stress of the Orowan dislocation loops around the precipitated particles against the successive emitted dislocations from Frank–Read (F–R) sources, i.e., the critical effective stress impeding F–R dislocations. In Fisher's investigation [136], the residual dislocation shear-loops around the particles were equivalently treated as the transformed strain prescribed in a classical Eshelby's inclusion problem [137] to deal with this stress state, which generates the average internal stress in the matrix to hinder the subsequent forward deformation. Brown et al. [138,139] proposed that the residual shear dislocation loops around the hard precipitates can impede the subsequent dislocation sliding in the matrix, resulting in formation of the source-shortening stress. The concept of the original Fisher's back-stress is referred by the so-called Orowan stress after the addition of inhomogeneous internal stress [139]. The concept of back stress was further extended by Brown and Stobbs [138], and Asaro [140] in the hardening model of dual-phase materials. They proposed that the incompatibility strains between the hard phase and the soft matrix can induce a long-range internal stress, which makes the dual-phase structure susceptible to reverse deformation. Later on, the concept was further extended to the long-range (internal) back stress between the soft and hard microdomains due to the micro-inhomogeneous strain during plastic deformation, which is the concept of back stress currently used [141,142]. In the earlier quantitative analysis of back stress by Cottrell [143], Orowan [144,145] and Embury [146], half of the difference between the forward and reverse flow stresses in Bauschinger testing was consistently used to characterize the magnitude of back stress, and hence the back stress was often called the Bauschinger stress. Wilson et al. [147] conducted an X-ray diffraction study on the non-relaxed lattice strains during deformation of a two-phase microstructure, and further demonstrated that permanent softening is ~1.9 times of the back stress when reverse loading reduces internal stress to zero. This experimental result was consistent with the

prediction of the aforementioned Orowan's model [144]. Furthermore, a large number of experimental results have shown that back stress plays a crucial role in the strain hardening, strengthening and mechanical properties of materials with non-homogeneous microstructures [121]. According to the Orowan's model [144], the macroscopic flow stress of materials with heterogeneous structure can be denoted as following:

$$\sigma_{flow} = \sigma_0 + \sigma_{forest} + \sigma_{back}, \tag{1}$$

where σ_0 is the initial resistance against occurrence of dislocation sliding, σ_{forest} is the dislocation resistance derived from the interactions between movable dislocations and forest dislocations, and σ_{back} is the long-range back stress due to the extra GND-induced hardening.

According to the definition of strain-hardening rate $\Theta = \partial\sigma/\partial\varepsilon$, when the changes in testing temperature and strain rate can often be ignored during the quasi-static tensile deformation [132], the Equation (1) can be rewritten as:

$$\Theta_{flow} = \Theta_{forest} + \Theta_{back}, \tag{2}$$

where Θ denotes the macroscopic strain-hardening rate, and Θ_{forest} and Θ_{back} are forest hardening rate and back-stress hardening rate, respectively. It can be seen that the back-stress hardening rate is essential for the enhancement of the overall strain-hardening rate of materials with HGS, and thus a scientific basis for exploiting and providing the potential hardening mechanism associated with monotonic plastic deformation has been proposed by Wu et al. [3].

We presented an analytical model to calculate the back stress based on the hysteresis loops observed in tensile loading-unloading-reloading test [53]. Upon tensile loading, yielding starts in larger grains, while small ones still remain elastic. The applied load will be transferred from large grains to small ones [148]. Upon unloading, the macroscopic stress decreases and the large grains are subjected to a compression stress when the small grains reach the completely unloaded state [122]. Upon subsequent compressive loading, the whole sample initially behaves elastically until the large grains enter in the plastic regime first in compression, a situation that will take place at a much lower absolute value compared to the initial tensile flow stress because of the pre-compression of large grains [53]. As a consequence, an asymmetry in the macroscopic forward (tensile) and reverse (compressive) yield stresses will occur (so-called Bauschinger effect [53,122]), and this effect characterizes the development of back stress [16,53]. Therefore, back stresses develop in terms of the load transferring from large grains to small ones, whereas the strain partitioning from small grains to large ones [148]. This is evidenced by the large width of hysteresis loops and high hardening rate due to back stress. Both the dynamic load transferring and strain partitioning along with the tensile straining lead to the increasing back stress [16,17,53].

Experimental studies have been conducted on the mechanical properties and deformation mechanisms of HGS in single-phase metals [16,18], dual-/multiple-phase alloys [20,21], and transformation-induced plasticity (TRIP)/twinning-induced plasticity (TWIP) steels [22,23], emphasizing on the back-stress-induced strengthening/hardening effects. Early research on metals with HGS started with synthesizing their microstructures [149,150]. Recently, great efforts and growing scientific interests have been focused on tailoring multi-scale hierarchical microstructures in a nanostructured matrix and achieving a synergistic strengthening/hardening from the combined effects of both grain refinement and extra hardening [14,16,123]. More recently, we [17] reported a simultaneous improvement of both strength and ductility in a single-phase fcc medium-entropy alloy (MEA) with dynamically-refined HGS. The MEA with HGS can be produced by a conventional heat-treatment of partial recrystallization annealing, which is currently a well-developed processing route at a low cost.

The grains can be efficiently refined for the MEA in situ during tensile deformation due to its low stacking fault energy (SFE) [151,152], thus reinforcing the HGS and increasing the back stress to promote strain hardening and hence uniform elongation. Compared with the MEA with homogeneous

UFG structure [86], the MEA with HGS has a significant higher uniform elongation and a similar flow stress. The dynamic grain refinement in HGS accommodates plastic deformation by facilitating the successive emission of SFs in new orientations (Figure 1a). This dynamic grain refinement induced plasticity (GRIP) effect by architecting HGS is therefore much like TRIP and TWIP in facilitating strain hardening and plastic flow [153,154]. In addition, the small grains are generated mainly at GBs and triple junctions of larger grains, where damage is more susceptible to initiate [1,17]. Thus, GRIP effect has beneficial influences on increasing fracture toughness, in addition to delaying plastic instability such as premature necking in tensile deformation. The dynamic grain refinement can also further reinforce the heterogeneity in HGS, and thereby increase the back-stress-induced strain hardening, suppressing the strain localization and prolonging the tensile uniform elongation. In consequence, the tensile uniform elongation of the MEA with HGS was enhanced up to 20% even when the yield strength was improved to above 1 GPa (Figure 1b) [17].
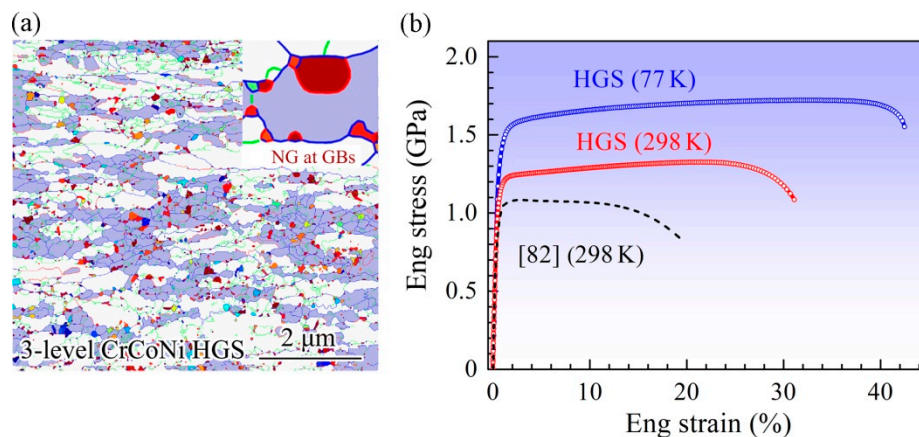

Figure 1. Microstructural characteristics and enhanced strength–ductility synergy of the MEA with HGS: (**a**) Architected HGS; (**b**) Engineering tensile stress–strain curves for the MEA with HGS under various testing temperatures. Adapted from [17].

Similar to the above processing approach, Slone et al. [87] produced another type of HGS with partially recrystallized microstructure in a similar MEA. Striking hysteresis loops are also observed not only in the sample with HGS at the early stage of plastic deformation, but also in the partially recrystallized sample with relatively homogeneous grain structure at end stage of uniform deformation. This result just further confirms that back-stress hardening plays a key role at a high stress level. It is well known that the dynamic generation of twin bundles during deformation and the consequent hardening can build a superior back-stress effect in TWIP steels with the conventional equilibrium CG structure [154]. Similarly, the role of architecting HGS for enhancing strain-hardening capacity in metals was well discussed in this paper. However, there are some obvious discrepancies between these two studies [17,154], though both the small NGs and the twin bundles are associated with the partial dislocations emitted from GBs and triple junctions. In Slone's case [87], a back stress can indeed be developed into a large magnitude due to the formation of the large amount of twin bundles during tensile testing in conventional CG microstructures. For our HGS, it should be noted that there are definitely deformation twins formed inside grains during tensile deformation, while these twins are the corner twins and these twins subsequently evolve into newly-formed NGs during further deformation [17]. In other words, twinning-induced back stress in our HGS should have played a smaller role in the strengthening and strain hardening during the tensile deformation.

It has attracted great interests for optimizing the strength–ductility synergy by tailoring the HGS. More and more experimental results have shown that the effect of back stress in providing extra strengthening and strain-hardening capacity for the materials with HGS. Although these studies have been conducted on the various HGSs with different morphologic and crystallographic features,

these microstructures do share one common characteristics: there is a dramatic difference in flow stress between different microdomains. This large difference in flow stress is often caused by huge heterogeneities in microstructure, crystal structure or composition in these domains. The domain sizes could be in the range of micrometers to millimeters, and the domain geometries can vary dramatically. It is indicated that heterogeneous microstructures can achieve a large accumulation of GNDs especially at the hetero-interfaces during inhomogeneous deformation, which in turn causes significant back stress, resulting in enhanced overall strain-hardening capacity. Therefore, how should the hetero-interfaces be designed? The hetero-interfaces should be designed to improve the constraints on soft domains exerted by the surrounding hard domains during plastic deformation, which is important for accommodating GNDs, bearing strain gradient, and inducing back stress [16,121]. The spatial distribution and morphology of hetero-interfaces, including geometric and microstructural characteristics, should have great influences on the mechanical behaviors of HGS. Thus, domain size, domain distribution, domain morphology, soft/hard domain volume fraction, and local discrepancies in yield strength and strain-hardening behavior between any two adjacent domains should be properly designed to optimize the mechanical properties of HGS [2,3].

2.3. Heterogeneous Lamella Structures

According to the above-mentioned strategies for inducing high back-stress, the heterogeneous lamella structure (HLS) presents a near-ideal heterogeneous structure due to both the high density of domain interfaces and the adjustable volume fractions for soft/hard domains in such microstructure [16,23]. Our recent results have shown that a commercially-pure Ti with HLS, which possesses the spatial distribution of the alternating hard and soft lamellae with their both widths ranging from a few to a dozen micrometers, presents enhanced tensile strength–ductility synergy (Figure 2a) [16]. Such Ti with HLS unprecedentedly surpasses its CG counterpart in strain hardening and consequently produces both larger ductility and higher strength (Figure 2b–d). The Ti with HLS was fabricated by asymmetric rolling followed by partial recrystallization annealing, which produced a strong local micro-hardness variation between the alternating hard and soft lamellae, as well as a slight macroscopic structural gradient with recrystallized grains of a few micrometers near the surface and recovered ultrafine-grains in the central region. In addition, the soft CG lamellae consisting of recrystallized grains are intermixed with the relatively harder UFG lamellae at microscopic scale. The HLS produces a strong internal mechanical incompatibility and long-range back stress at macroscopic scale from the surface to the center as well as at microscopic scale between adjacent lamellae (Figure 2e). During the deformation of HLS, the GNDs are gradually generated and blocked by hetero-interfaces to induce back stress (Figure 2f). This extra strain hardening induces even higher overall strain hardening in Ti with HLS than that in CG Ti, which is usually believed to be impossible [16].

This enhanced tensile properties for HLS as compared to these for uniform structure can also be attributed to the local variations in the hardness between alternating recovery and recrystallized lamellar domains [16,53]. This hardness difference needs to be large enough to generate local incompatibility of plastic deformation and local extra hardening for improvement in global hardening. In a summary, larger local gradients and higher local GNDs render the better mechanical performances, such as yield strength, strain-hardening rate, and uniform elongation [16,26,53]. The local variation in hardness in the deformed state is small, but it is enhanced after recovery and partial recrystallization annealing. This has been verified by micro-hardness testing on recovered and recrystallized lamellae [16]. The best combination of strength, strain-hardening rate and uniform elongation should be associated with the optimized difference in hardness between soft and hard lamellae. Moreover, the spatial distribution of the alternating hard and soft lamellae, rather than a random distribution of irregular grains and soft/hard domains, should have better performance on mechanical properties [3,16].
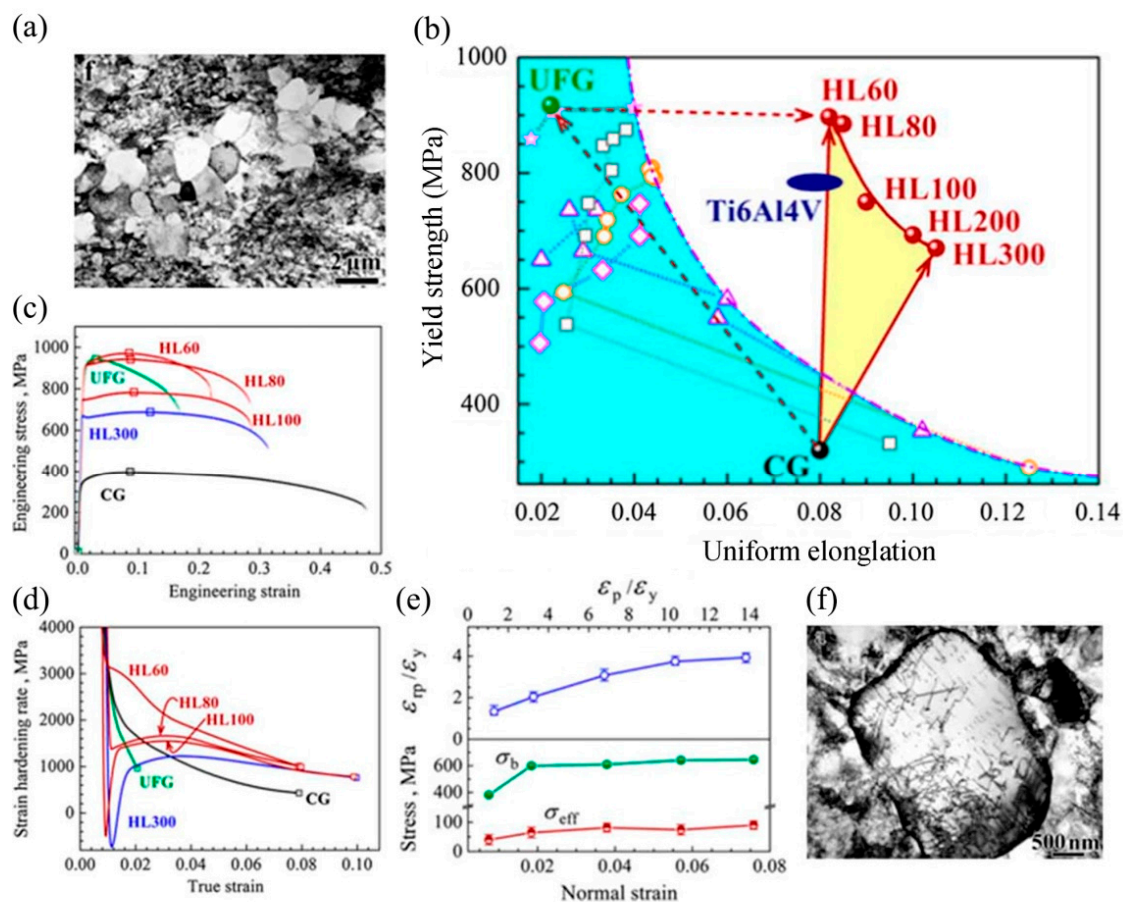
Figure 2. Unprecedented strengthening and extra strain-hardening in Ti with heterogeneous lamella structure (HLS): (**a**) Microstructural characteristics of HLS; (**b**) Outstanding tensile properties of Ti with HLS; (**c**) Engineering tensile stress–strain curves for various samples; (**d**) True strain hardening rate vs. true stress for various samples; (**e**) Back stress hardening behaviors for Ti with HLS; (**f**) Dislocation pile-ups at hetero-interfaces. Adapted from [16].

Recent studies on copper/bronze laminates by Huang et al. have revealed possible existence of an optimum layer thickness for the best mechanical properties [25,155]. In-situ microstructural examinations during tensile deformation revealed pile up of high-density GNDs at the hetero-interfaces. This result suggests that interface-affected zone likely exists and has a width of a few microns, which is the key factor to maximize the back-stress hardening. When the spacing between the hetero-interfaces is large, the density of GNDs should be low. While too small spacing would cause the overlapping of the distributions of GNDs for neighboring interfaces, resulting in decreasing strain hardening and tensile ductility. Thus, a proper spacing between the hetero-interfaces has been identified to be about 15 μm for generating the best tensile properties for the copper/bronze laminates [25].

2.4. Heterogeneous Phase Structures

The transient strain-hardening phenomenon has been experimentally observed in the various metals and alloys with either a simple homogeneous grain microstructure or a complex multi-scale hierarchical grain/phase microstructure [14,16,17,28]. In simple metals, this phenomenon is generally attributed to the heterogeneous distributions of GBs and dislocation substructures, such as dislocation cells and dislocation walls [156,157]. However, the transient phenomenon has not yet been completely understood in heterogeneous structure [14,16,17], which is much more complex than that of homogeneous materials because of discrepancy in deformation behaviors between neighboring microdomains/phases. To better understand this issue, we conducted a synchrotron-based in-situ

tensile testing on a Fe-16Mn-10Al-0.86C-5Ni high specific strength steel (HSSS) with heterogeneous microstructure, in order to clarify the possible micro-mechanisms underlying the elasto-plastic deformation and back-stress hardening of this heterogeneous phase structure (HPS). This investigation would also help for understanding of the transient strain-hardening phenomena in materials with heterogeneous microstructure [28].

The HSSS with heterogeneous microstructure shows a remarkable feature of the elasto-plastic deformation behavior, resulting in a pronounced hardening transition on the stress–strain curves during an early stage of deformation (Figure 3a) [28]. This phenomenon can be attributed to inhomogeneous deformation occurring in this dual-phase steel because of the microstructural heterogeneities and long-range back stresses arising from plastic incompatibilities between alternating-distributed phases with different responses of mechanical properties. In fact, a composite-type elasto-plastic deformation prevails in most high strength steels [14,16,17,28,53]. This is due to the plastic deformation heterogeneity between the constituents, phases and grains with different mechanical responses and even orientations relative to an externally applied stress. This will lead to the presence of long-range internal stress, i.e., back stress, which evolves with applied strain because of intra- and inter-granular variations of plastic strains, and the evolved back stress has a strong impact on the strain-hardening behaviors and macroscopic mechanical properties [29,158,159]. It is a great challenge to investigate the strain hardening behaviors associated with the back stress in the HPS since it is a complex interplay between individual phases due to the presence of hetero-phase interfaces [28]. More importantly, both the load redistribution and strain partitioning will take place in HPS during plastic deformation [28]. These effects enable not only high capacity of strain hardening but also a large uniform elongation in a composite-type microstructure [28,122].
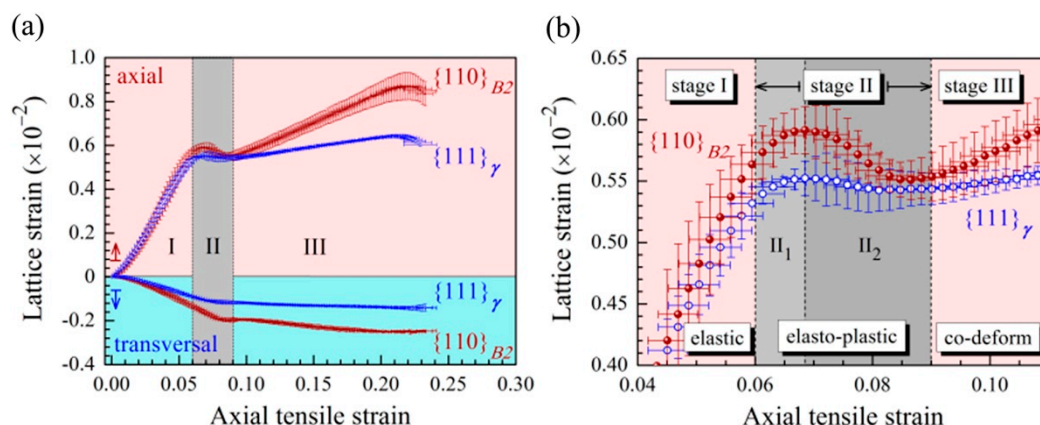

Figure 3. In situ x-ray diffraction measurements for the HSSS with HPS during tensile deformation. (**a**) Lattice strains in both hard B2 phase and soft austenitic matrix vs. applied tensile strain; (**b**) Close-up view for the transient region. Adapted from [28].

Upon the applied tensile strain, the axial lattice strains in both soft austenitic matrix and hard B2 phase can roughly be divided into a three-stage evolution, i.e., elastic deformation, elasto-plastic transition, and plastic co-deformation up to overall necking (Figure 3b) [28]. In the stage of elastic deformation, both the axial lattice strains of austenitic matrix and B2 phase coincide well and increase linearly. During the elasto-plastic transition stage, the lattice strain of austenite firstly deviates from linearity, while the lattice strain of B2 phase still increases linearly. With the further tensile strain, a rapid drop in lattice strains of both austenite and B2 phases is observed clearly. In the stage of plastic co-deformation, the axial lattice strains of both austenitic matrix and B2 phase begin to rise nonlinearly, but with different slopes. Moreover, the transition process can be subdivided into two sub-stages according to the plastic yielding first in austenite and soon afterwards in B2 phase. In the first sub-stage (II_1), a grain-to-grain yielding takes place first in soft austenitic matrix due to varying Schmid factors and strain-hardening behaviors of individual austenite grains. During the second

sub-stage (II₂), a rapid drop of lattice strain in B2 phase appears, indicating that B2 phases start to yield for accompanying the decline in load shedding from softer austenite to harder B2 phase through hetero-phase interfaces.

The unique up-turn hardening in the stress–strain curves observed in HPS can therefore be attributed to the nature of elasto-plastic transition [28,122]. Under tensile loading, soft phase will deform plastically first. However, they are constrained by still elastic-deformed hard phase such that dislocations in soft one are piled up and blocked at hetero-phase interfaces. GNDs will also be generated at hetero-phase interfaces due to the plastic strain incompatibility [28,121]. This produces the back stresses to make it difficult for dislocations to slip in soft phase until the surrounding hard phase starts to yield at larger applied strain. As a consequence, both inter-phase back stresses and intra-phase back stresses occur, which are attributed to the progressive yielding of grains and phases [28,129]. This is the reason why a much high back-stress hardening is visible exactly at the transient stage (elasto-plastic deformation stage). The high strain hardening is therefore originated from both back-stress hardening and forest dislocation hardening in both phases. Moreover, once the B2 phase yields, rapid relaxation of elastic stresses and strains on the hetero-phase interfaces causes a rapid stress-drop [28,129]. Afterwards, the macroscopic strain-hardening rate resumes to rise up gradually as a consequence of the back stresses resulting from the strain incompatibility together with rapid dislocation multiplication in both phases [28]. The development of the back stress during plastic deformation of two-phase microstructure due to dynamic strain partitioning and yield stress mismatch was also described in other research [123,124,129,154].

In fact, back stress strengthening/hardening has also been reported in nanocomposites [122], dual-phase alloys [28] and TRIP/TWIP steels [160]. He et al. [23] have developed another similar HPS coupled with V-containing nanoprecipitates in medium-Mn steel, i.e., the so-called deformed and partitioned (D&P) steel [23]. Based on the experimental observations and theoretical analysis, they have proposed that the high dislocation density in the D&P steel not only increases the yield strength, but also enables a large ductility by the glide of existing mobile dislocations and by the controlled release of TRIP effect, resulting in an ultrahigh yield strength reached to above ~2 GPa, 50% higher than that of the conventional high-strength steels, together with a comparable uniform elongation. Besides, a Lüders-like nonuniform deformation behavior is exhibited in such D&P steel during tensile deformation, and the more in-depth mechanisms have not yet been revealed.

3. Gradient Structure

Materials from nature and biological systems, such as bamboos, teeth and seashells, have been found to have gradient structure from the surface to the interior and exhibit exceptional mechanical properties [30]. Learning from nature, mankind has designed gradient structure in engineering materials to achieve novel and superior physical and mechanical properties [34–65]. These mechanical properties include uniaxial tensile properties, dynamic properties and fatigue properties. For gradient structured metals with exceptional mechanical properties, the strength/hardness generally shows a gradient along the depth. As a result, the microstructures (grain size, phase fraction, twin volume fraction/twin thickness, and texture/orientation) display an apparent gradient along the depth.

3.1. Fabrication Methods

In 1999, a concept of surface nanocrystallization on metals and alloys was introduced for the first time [35], a gradient structure was produced by surface mechanical attrition treatment (SMAT) and nanostructured (NS) grains were formed at the surface layer by repetitive severe plastic deformation (Figure 4a). In 2003, the SMAT technique was utilized to enhance the efficiency of nitriding process [38]. The grain size was refined and a fraction of GBs was increased in the surface layer during SMAT. Thus, the nitriding kinetics of the surface treated iron were significantly improved since GBs can be considered as well-known high ways for diffusion processes [38]. Later on, another surface nanocrystallization technique, surface mechanical grinding treatment (SMGT) at cryogenic temperature Figure 4b, has

been used to fabricate a gradient nano-microstructured surface layer on copper and the grain size at the topmost surface was as small as 22 nm [41].
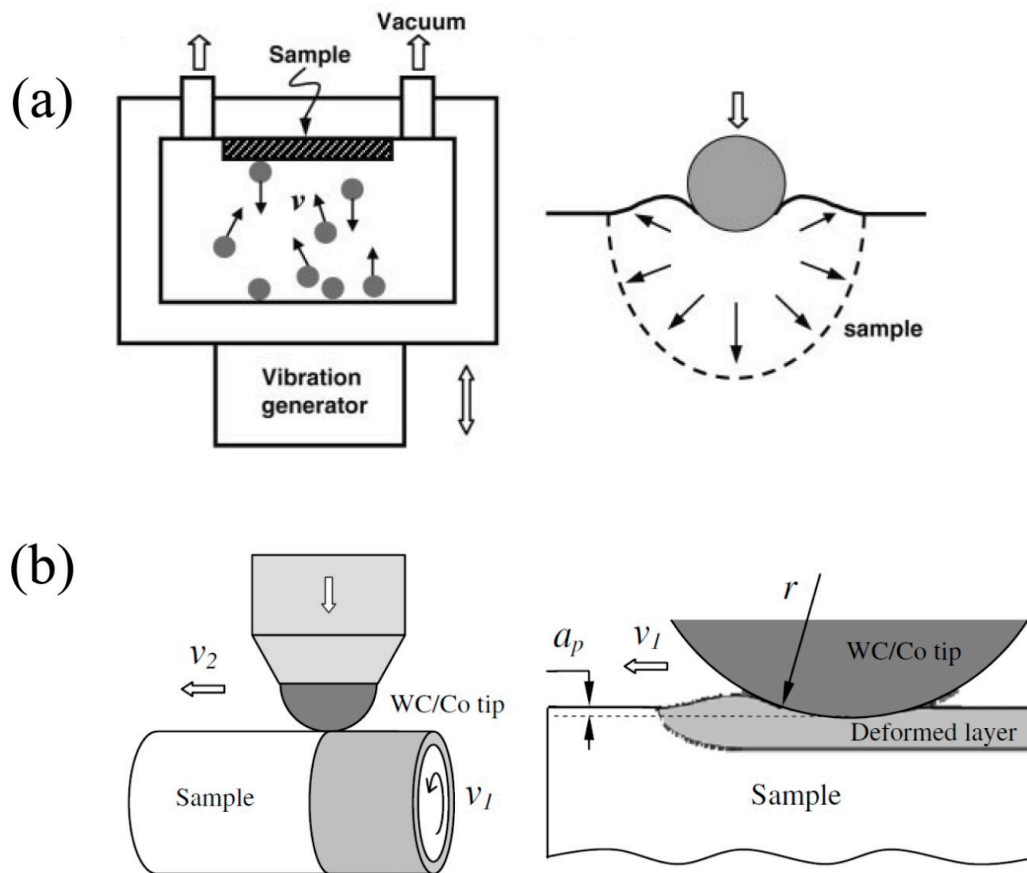

Figure 4. Schematic illustrations of SMAT (**a**) and SMGT (**b**) techniques. Adapted from [38] and [41].

3.2. Tensile Behaviors of Gradient Grained Structures

The tensile properties of gradient structured metals were started to be investigated since 2008. A new microstructure, multiple layered structure with gradient grain size in each layer, has been obtained by SMAT technique and subsequent warm co-rolling technology, and excellent tensile properties have been revealed in this new microstructure [40]. The compression residual stress and deflection of cracks by the interface between the nanostructured layers have been found to play important roles for achieving high ductility in this periodically layered gradient structure [40]. As we know, NC metals can have much higher strength when compared to their CG counterpart, while NC metals are believed to be intrinsically brittle under uniaxial tensile loading. When the NC copper film is confined by a CG layer in the gradient structure, strain localization can be suppressed and large uniform tensile ductility can be achieved [42]. The intrinsic deformation mechanisms for large tensile plasticity of NC copper surface layer in gradient structure have been revealed by Fang et al. [42] for the first time, and the substantial grain growth by mechanically-driven GB migration process has been proposed to be the dominant plastic deformation mechanism of this gradient NS layer (Figure 5). These "in-situ" coarsened grains help to regain strain hardening and dislocation plasticity in the surface layer. More recently, a critical grain size of 165 nm was identified in the gradient structured copper during uniaxial tension, tension-induced softening was observed for grains smaller than this critical grain size while tension-induced hardening was found for grains larger than this critical grain size [46]. The observed softening was attributed to the grain growth in the small grains while the strain-induced hardening in the large grains was due to dislocation multiplication and formation of dislocation walls/cells.
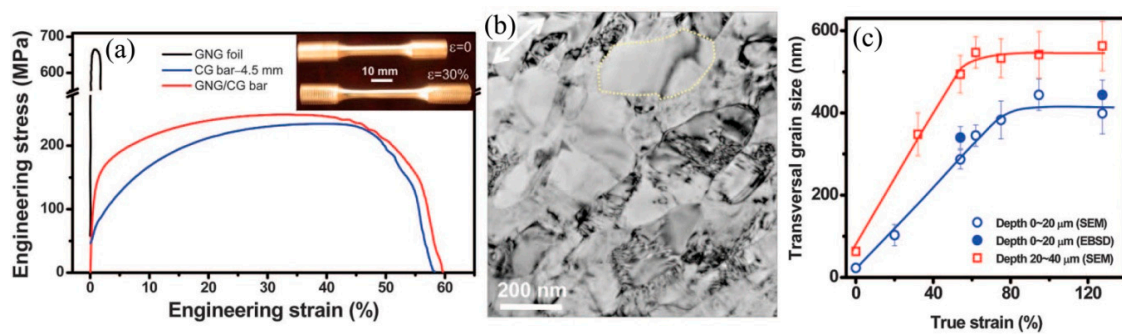
Figure 5. Tensile properties and corresponding deformation mechanisms of gradient grained copper: (**a**) Engineering stress–strain curves; (**b**) TEM image of the top layer after a true tensile strain of 33% showing "in-situ" coarsened dislocation-free grains; (**c**) Variation of average grain sizes with applied tensile strain for the gradient layer. Adapted from [42].

Using the same SMAT technique, we have produced a gradient structure in an IF steel and large tensile ductility was achieved in the NS surface layer of IF steel without apparent grain growth when confined by the CG substrate [14]. These observations suggested that the varying propensities for flow instability between different layers in the gradient structure can induce stress-state change to suppress the strain localization in the NS surface layer [14]. Extra synergic strengthening and extra hardening were also induced by strain gradient to help tensile ductility, and the strain gradient was due to the mechanical incompatibility between different layers during the elasto-plastic stage and the co-deformation stage in the gradient structure [14,15]. An obvious up-turn for strain hardening rate was also observed due to the stress-state change and the strain gradients (Figure 6). As we know, the strain gradients are generally accommodated by the pileup of GNDs at the interfaces, which in turn generates long-range back stress between the hard NS surface layer and the soft CG core. We proposed a simple equation to calculate back stress from the tensile unloading-reloading hysteresis loop based on its deformation physics, and also reported strong back stress strengthening/hardening in the gradient structured IF steel [14]. Using the tensile load-unload-reverse compressive load testing, we also reported extraordinarily larger Bauschinger effect in the gradient structure compared to the CG counterpart and proposed to use the reverse yield softening as a quantitative parameter to represent the Bauschinger effect [53]. This parameter can be utilized to evaluate the magnitude of back stress hardening for exceptional tensile properties in heterogeneous materials.

Moreover, we reported an "in-situ" evolution of the induced strain gradients in a gradient-structured metals during uniaxial tension [57]. We found that the lateral strain gradients increase with increasing applied tensile strain, and the strain gradients increase faster and the back-stress hardening plays more important role at the elasto-plastic transition stage. It is well known that NS metals typically fail soon after yielding under uniaxial tensile loading, starting with strain localization. Thus, low tensile ductility in NS metals is ascribed to strain localization, so one always tries to avoid localization, but never think about how to utilize it. We illustrated for the first time how to adopt the good point of localization, i.e. collecting vast strains for ductility, and to avoid its shortcoming, i.e. fast instability, by stabilizing localized shear band in the gradient structure [63]. This novel strategy overturned our traditional understanding for strain localization. We exhibited for the first time that localization may induce ductility, instead of catastrophic failure. This enhanced ductility in the gradient structure was fulfilled by the shear band delocalization: shear bands were initiated soon after yielding in the NS surface layer, while were delocalized by propagating along the gage length during the tensile loading, and synergistic work hardening was induced by back stress hardening from the strain gradients in both the axial and depth directions [63].
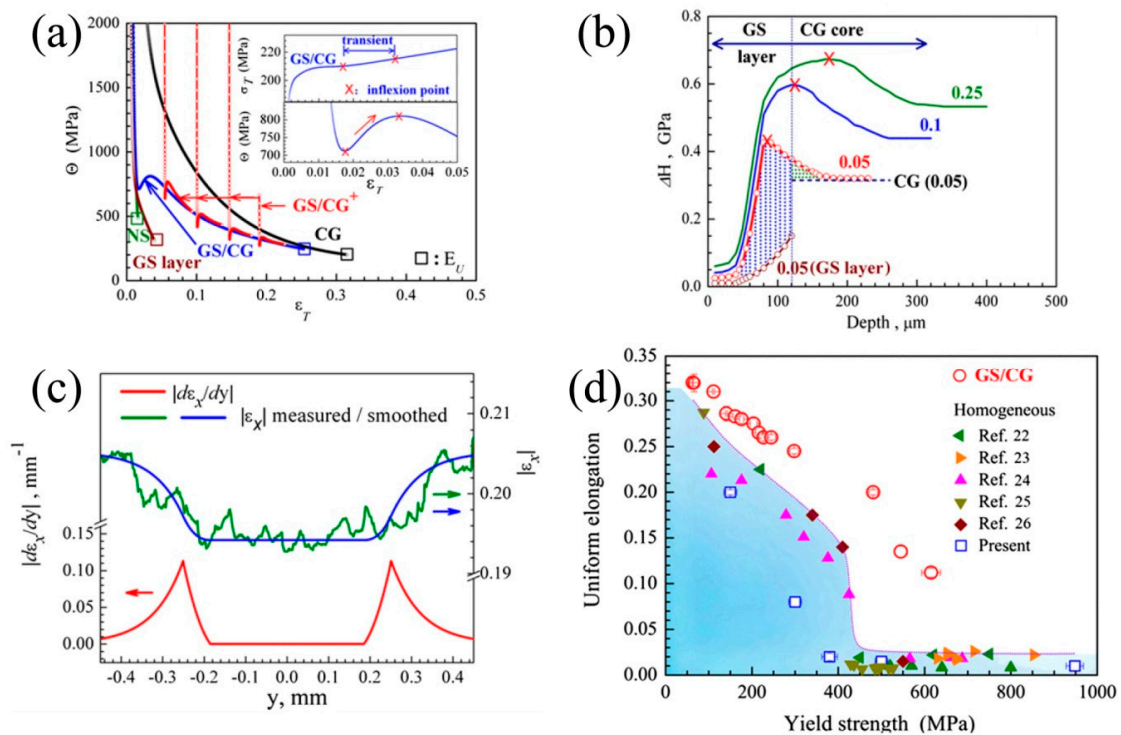
Figure 6. Tensile properties and extra strain hardening mechanisms of gradient grained IF steel: (**a**) Strain hardening rate vs. true strain curves; (**b**) Extra strain hardening by gradient structures; (**c**) Distributions of lateral strain and strain gradient along the depth; (**d**) Superior tensile properties of gradient structures over homogeneous counterparts. Adapted from [14].

3.3. Tensile Behaviors for Other Types of Gradient Structures

Besides the gradient structure with grain size gradient, other types of gradient structures (i.e., gradients for phase fraction, twin volume fraction/twin thickness, and texture/orientation) also showed great potential for achieving superior tensile properties [27,47,51,56,59]. Wei et al. [47,51,56] applied pre-torsion deformation to a cylindrical twinning-induced plasticity steel sample to generate gradient of twin volume fraction along the radial direction (Figure 7). They found that the yield strength of the gradient twinned structure can be doubled without sacrifice of tensile uniform elongation compared to the untreated CG sample, evading the strength–ductility trade-off dilemma. The enhanced tensile properties in the gradient twinned structure have been attributed to two points: (i) the formation of a gradient hierarchical nanotwinned structure during the pre-torsion deformation and the subsequent tensile loading; (ii) this hierarchical nanotwinned structure is generated in the sequential torsion and tension deformation by activating different twinning systems. Cheng et al. [13] fabricated a dual gradient structure of grain size and twin thickness by direct-current electrodeposition method. This dual structural gradient was found to show superior work hardening and strength that can exceed those of the components of the gradient structure. The enhanced tensile properties have been attributed to a unique patterning of ultrahigh densities of dislocations in the grain interiors: bundles of concentrated dislocations, a special type of GNDs (Figure 8). These bundles of concentrated dislocations were induced due to the nature of gradient, were not available in the homogeneous samples [64].
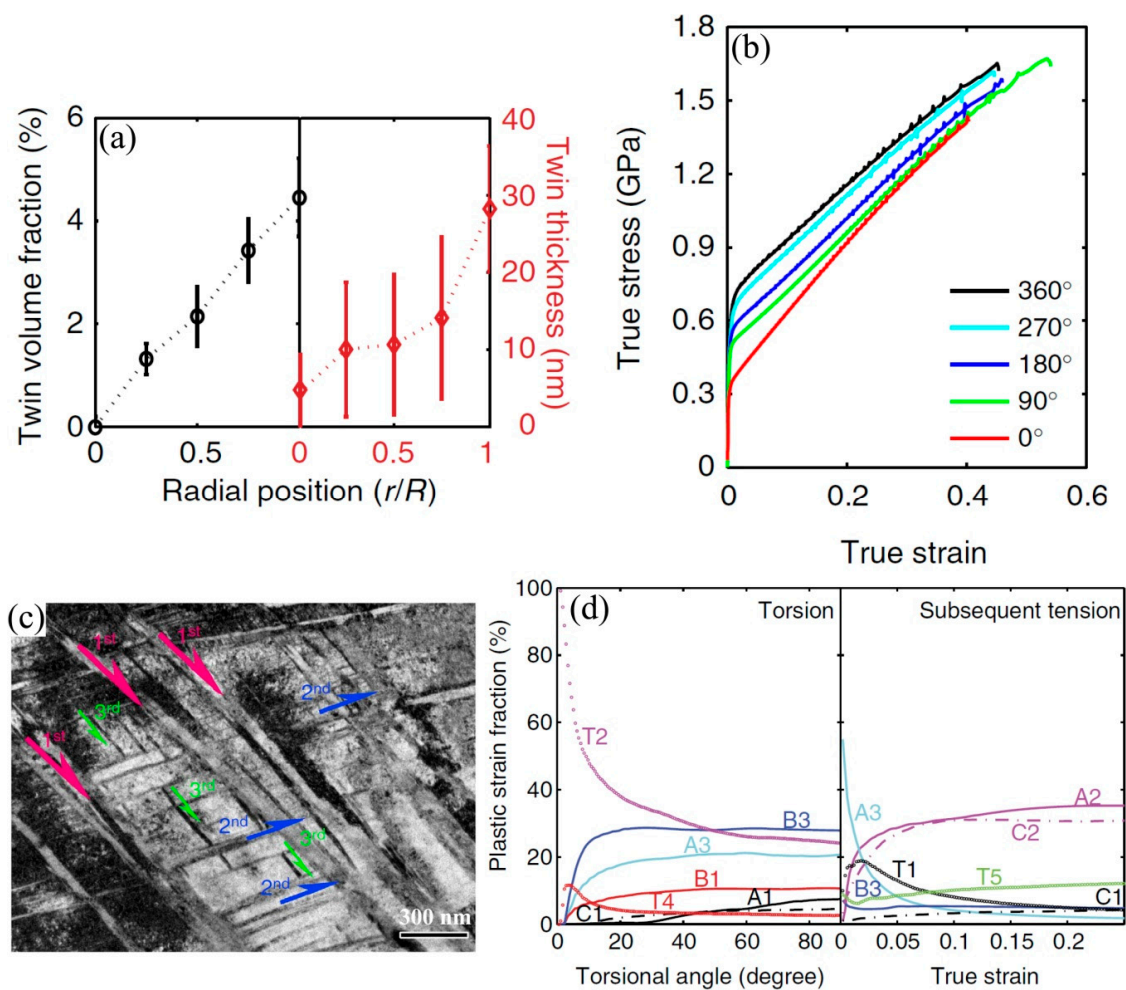
Figure 7. Tensile properties and corresponding deformation mechanisms of a TWIP steel with gradient twinned structure: (**a**) Twin volume fraction and twin thickness distributions along the radial direction; (**b**) True stress–strain curves; (**c**) Hierarchical twin structures formed during the pre-torsion deformation and the subsequent tensile loading; (**d**) Activated different twinning systems in the sequential torsion and tension deformation. Adapted from [47].

We generated dual gradients with respect to grain size and martensite phase fraction in a TRIP steel by SMAT technique [27]. A design strategy was reported to combine the both benefits from gradient structure and TRIP effect, and the reported TRIP-gradient steel was found to take advantage of both mechanisms, prolonging the TRIP effect to large strains [27]. Significant heterogeneity for strength exists not only macroscopically between the hard surface layer and the soft center layer, but also microscopically between the soft austenite domains and the hard martensite walls. Thus, the martensitic transformation was found to be triggered successively along the depth with tensile loading due to the strain partitioning between soft and hard areas, enabling the martensitic transformation to last to a larger tensile strain. As a result, the reported TRIP-gradient steel displayed an excellent combination of high strength and ductility due to both the dynamic strain partitioning and the TRIP effect. The SMAT technique was also utilized to fabricate the dual gradient structure of grain size and orientation in a Mg alloy [59]. The stronger strain hardening and higher tensile ductility were attributed to the pyramidal dislocations activated in the whole sample and higher dislocation density induced by grain-size gradient in the dual gradient structure.
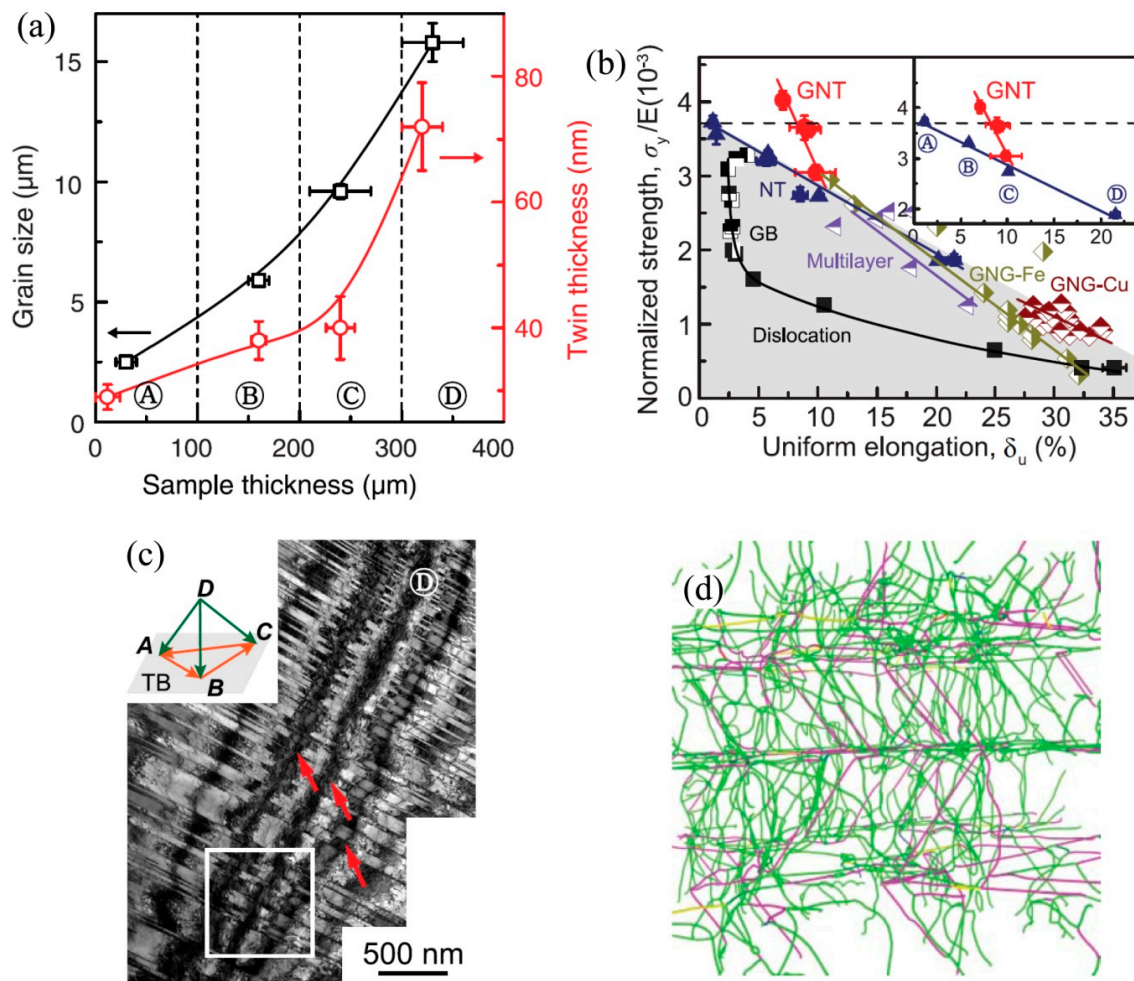
Figure 8. Tensile properties and corresponding deformation mechanisms of gradient nanotwinned copper with highly tunable structural gradients: (**a**) Grain size and twin thickness distributions along the thickness; (**b**) Tensile properties; (**c**) Deformation microstructure of gradient nanotwinned structure at 1% strain showing bundles of concentrated dislocations; (**d**) High density of dislocations in the bundles of concentrated dislocations revealed by MD. Adapted from [13].

3.4. Dynamic Behaviors of Gradient Structures

It is well known that the plastic flow behaviors and the observed flow stresses in metals and alloys highly depend on the loading rate. The materials display dramatically different mechanical behaviors at high strain rates due to the substantial adiabatic temperature rise, thermal softening, inertial and strain rate effects, and the formation of adiabatic shear band (ASB) compared to those at quasi-static strain rates [52,58,65]. A few studies have been conducted to focus on the dynamic behaviors of gradient structures [43,52,58]. Jérusalem et al. [43] have conducted a series of ballistic tests on the gradient structures to build two length scales as optimization parameters for ballistic performance: one is the intrinsic length scale (the finest grain size and the grain size gradient), and the other one is the extrinsic length scale (the thickness of the samples). Proper choice of these two length scales can lead to the best ballistic properties. Strain hardening behaviors and strain rate sensitivity (SRS) of gradient grained iron under compressive loading over a wide range of strain rates (5×10^{-4}–10^4 s^{-1}) have been investigated in our recent work [52]. The gradient grained iron was found to show apparent strain hardening behaviors at all investigated strain rates, and the extra hardening at all strain rates were believed to be due to the back stress hardening induced by the plastic deformation incompatibility between different layers in the gradient structures. The dynamic SRS of

the gradient grained iron was found to be slightly higher than that of the CG counterpart, which is controversial to the general observation that SRS should decrease with decreasing grain size for BCC metals [161]. This enhanced SRS in the gradient structure was attributed to the additional increase in dislocation density by the GNDs associated with the strain gradients and the back stress hardening. The dynamic shear behaviors of a gradient structured TWIP steel have been investigated in our recent paper [58]. The gradient structured TWIP steel was observed to have better dynamic shear properties over the homogeneous counterparts, which can be attributed to the suppression of ASB nucleation and propagation in the gradient structure (Figure 9). The propagation velocity of ASB in the gradient structures was found to be one order of magnitude lower than that in the homogeneous counterparts. Moreover, the well-known maximum stress criterion on ASB nucleation for homogeneous materials was found to be no longer valid for the gradient structures.
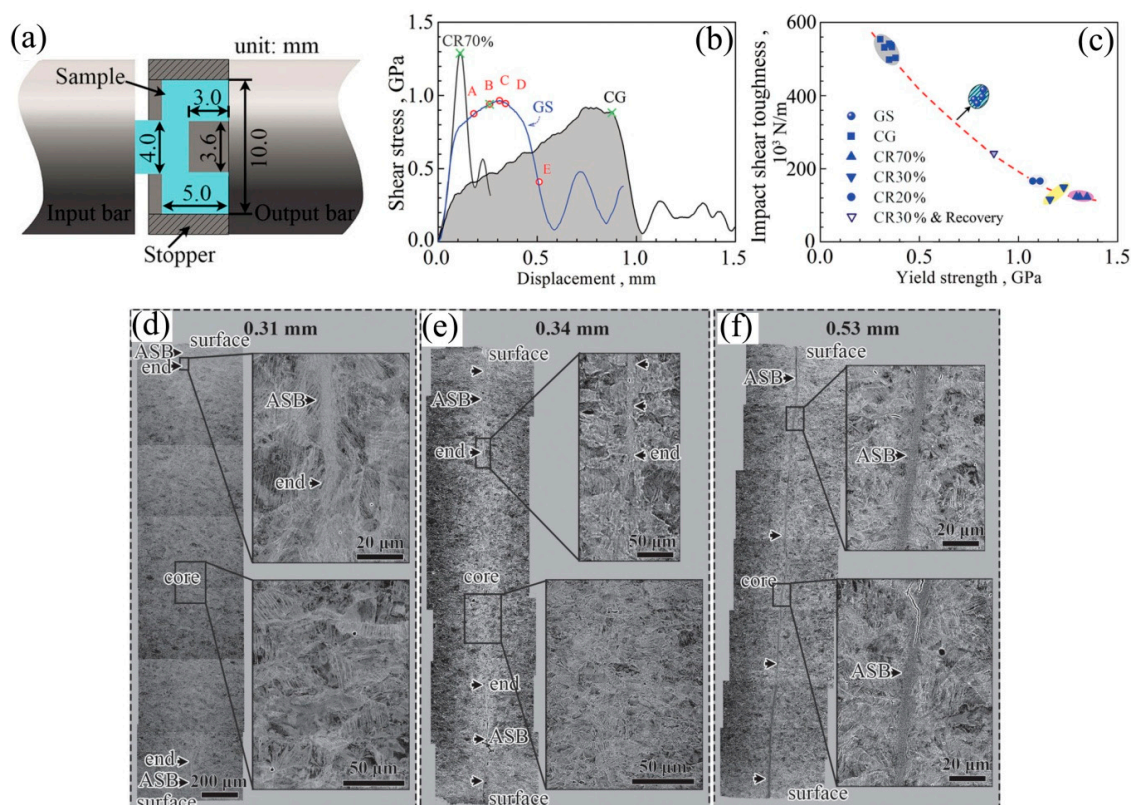

Figure 9. Dynamic shear properties and corresponding deformation mechanisms of gradient structure: (**a**) Set-up of dynamic shear experiments in Hopkinson bar; (**b**) Shear stress-shear displacement curves; (**c**) Impact shear toughness vs. dynamic shear yield strength; (**d**–**f**) Propagation process of ASB from the surface to the center. Adapted from [58].

3.5. Fatigue Behaviors of Gradient Structures

In structural applications, most materials and components fail under cyclic loading, thus the fatigue behaviors of metals and alloys have attracted extensive interests, in which a few papers have focused on the fatigue mechanisms of the gradient structures [39,45,49,61]. Roland et al. [39] have investigated the fatigue behaviors of a gradient-structured 316L stainless steel, and significant improvement of the fatigue limit has been achieved in the gradient structure. The fatigue properties can be further improved by a short post-annealing treatment, which can be attributed to a recovery at the GBs leading to a reduction of the internal stress (Figure 10). The similar fatigue behaviors have also been observed in a gradient structured martensitic stainless steel [45], the torsion fatigue strength of the gradient structure is 38% higher than that of the original material and an additional 8% increment in fatigue strength was achieved after a post-annealing treatment. The enhanced fatigue properties

can be attributed to the formation of the gradient structure with a hard surface layer with a high structural homogeneity. Huang et al. [49] have investigated the fatigue behaviors of an AISI 316L stainless steel with gradient structures and found that the fatigue strength of the gradient structure is significantly improved in both the low- and high-cyclic fatigue regimes compared to that of the original material. Moreover, the fatigue ratio (the fatigue limit divided by the ultimate tensile strength) was also apparently elevated in the gradient structure. Due to the hard surface layer, these enhanced fatigue properties can be attributed to the suppression of the initiation of cracks and accommodation of a remarkable cyclic plastic strain amplitude. Mechanically driven abnormal grain growth has been observed in a gradient grained copper under strain-controlled cyclic loading [61]. This abnormal grain growth was observed to start from the ultrafine grained subsurface layer and eventually move to the NS top surface layer with increasing cycles. They have attributed the enhanced fatigue properties of the gradient structured copper to the abnormal grain coarsening and the formation of dislocation patterns, which in turn accommodate the cyclic plastic strain and postpone the formation of extrusions/intrusions at the surface for improving the cyclic properties.
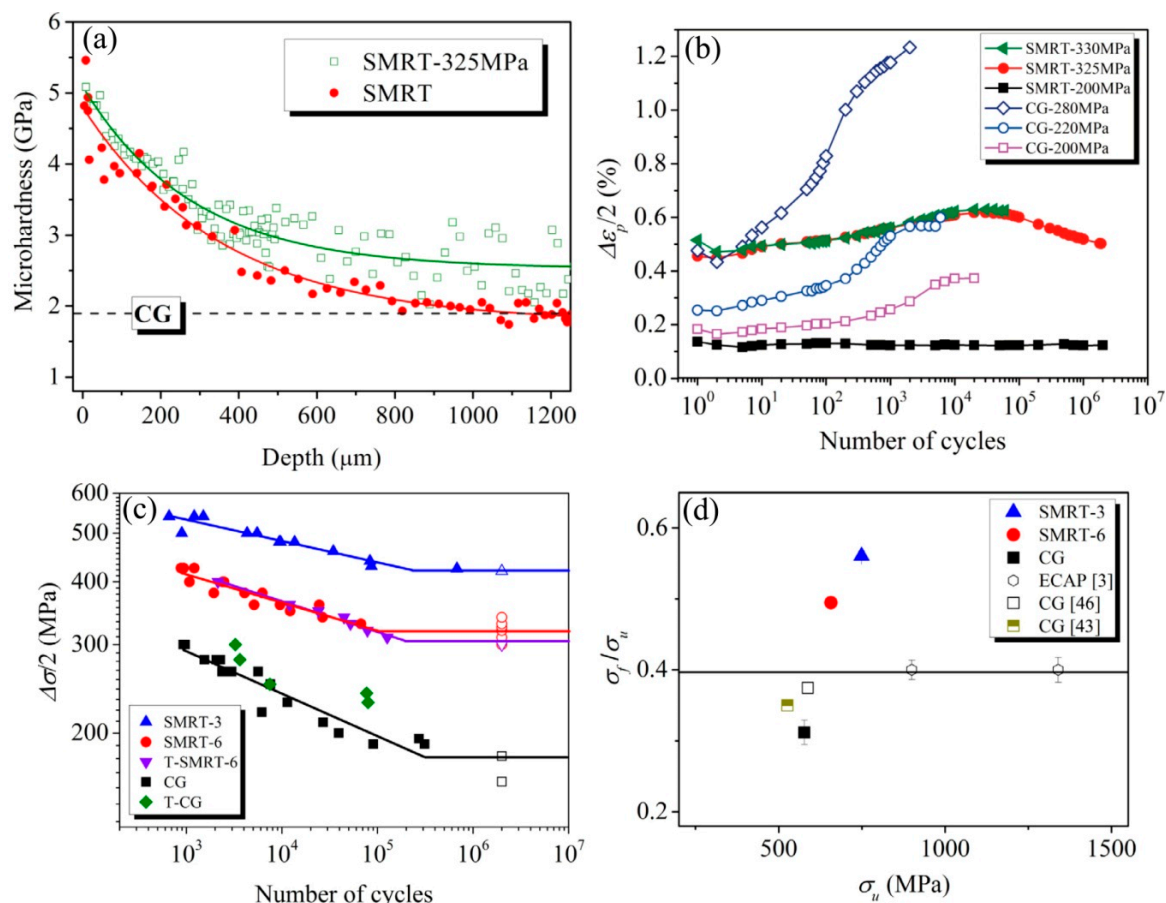

Figure 10. Fatigue behaviors of an AISI 316L stainless steel with gradient structure: (**a**) Distributions of microhardness along the depth for different samples; (**b**) Cyclic deformation curves of the CG and the gradient structured samples at different stress amplitudes as indicated; (**c**) S-N curves of different samples; (**d**) Correlation between the tensile strength and fatigue ratio (adapted from [49]).

3.6. Theoretical and Numerical Work for Gradient Structures

The above-mentioned experimental evidences have shown that the enhanced mechanical properties (uniaxial tensile, dynamic and fatigue) can be achieved by the gradient structure, while the detailed mechanisms underlying the observed mechanical behaviors still need further investigations and how the mechanical properties can be optimized in the gradient structure need be clarified

by theoretical and numerical modeling. In the past decade, several approaches (i.e., dislocation density-based continuum plasticity modeling [48,54,55], dislocation mechanism-based size-dependent crystal plasticity modeling [64], Crystal plasticity finite element modeling [65] and molecular dynamics (MD) simulation [60]) have been utilized to understand the strengthening and strain hardening behaviors. Li et al. [48,54] have developed a dislocation density-based continuum plasticity model to reveal the extra strain hardening behaviors in the gradient structure of IF steel, in which the nonuniform deformation of the lateral surface, the interaction of different layers along the depth, GNDs and back stress were considered (Figure 11). A simple physical law with two dimensionless parameters has been established to build the correlation between the strong extra strain hardening and the nonuniform deformation of the lateral surface, and these two parameters can be determined by experimental data. Based on the dislocation density-based continuum plasticity model, the strain hardening rate up-turn as observed in experiments was well reproduced and a strength–ductility map was plotted, in which the gradient structure clearly shows much more superior mechanical properties to their homogeneous counterparts. They have attributed the high strain hardening rate of the gradient structure to the generation of abundant GNDs in the NS surface layers through analyzing the evolutions of GNDs density distribution and back stress. Zeng et al. [65] have investigated the mechanical behaviors of the gradient grained copper using crystal plasticity finite simulations. They revealed both gradients of stress and plastic strain in the cross-section of the gradient grained copper under uniaxial tensile loading, these spatial gradients were found to be due to the progressive yielding of each layer along the depth during the tensile deformation. GNDs can be generated by these plastic strain gradients, which is contrast to the widely studied strain gradient plasticity induced by nonuniform deformation (i.e., torsion, bending and indentation at small scales).
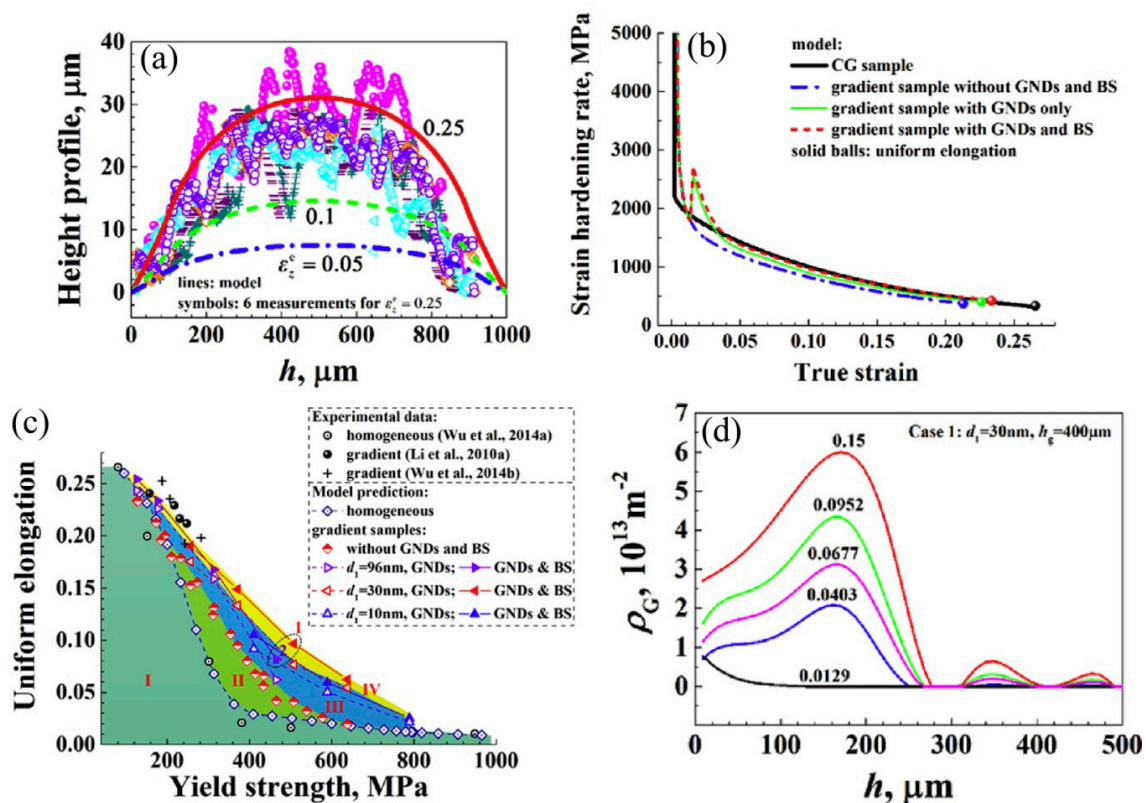

Figure 11. Dislocation density-based continuum plasticity modeling for gradient structure: (**a**) The predicted height profile on the lateral surface of a gradient IF steel and comparison with experimental data; (**b**) The predicted strain hardening rate and comparison with experimental data; (**c**) Strength–ductility maps of the gradient IF steel considering GNDs and back stress; (**d**) The predicted GNDs density distributions for one case. Adapted from [54].

Lu et al. [64] have incorporated multiple dislocation evolution, damage evolution, and mechanically-driven grain growth into a dislocation mechanism-based size-dependent crystal plasticity model to predict the tensile behaviors of the gradient grained copper. The simulated results have revealed the strengthening and the strain hardening mechanisms based on the spatial distribution and the evolution of microstructure and damage and have demonstrated the ability to optimize the strength and the ductility of the gradient grained copper. Zhu et al. [55] have developed a mechanism-based dynamic plastic model to describe the strain-rate dependent flow behaviors in gradient nanotwinned austenite stainless steels. These theoretical simulation results have indicated that the dynamic properties of the gradient nanotwinned austenite stainless steels are highly sensitive to the twin spacing and the twin volume fraction, and this mechanism-based dynamic plastic model can be used to well predict the plastic response of the gradient nanotwinned metals under a wide range of strain rates. Lin et al. [60] have combined experimental observations and molecular dynamic simulations to reveal the optimal grain size distribution profile of the gradient structure. The results have indicated that the surface roughening of CGs and strain localization of NS grains can be effectively suppressed by the interaction between CG grains and NS grains, resulting in the observed strong strain hardening and the superior uniform elongation. The aforementioned theoretical and numerical simulations have provided not only promising methodologies of producing gradient structure with optimizing mechanical properties, but also models for understanding the deformation mechanisms in the gradient structures.

4. Nanotwinned Structure

Nanotwinned (NT) structure has been proven to be a useful strategy for achieving ultra-high strength with acceptable ductility in face-centered cubic (FCC) metals, especially in FCC metal and alloys with low SFE. Twin boundaries (TBs) in crystalline materials are efficient and easy-controlled interfaces that can interact with dislocations, similar to GBs [12]. TBs can be introduced into grains during deposition processing (so-called growth twins), plastic deformation (so-called deformation twins) or annealing of deformed structures (so-called annealing twins). Due to the lower energy, TBs usually exhibit much higher thermal and mechanical stabilities compared with high-angle GBs [66]. It was shown that introduction of twins for designing material structures offers substantial strengthening while preserving acceptable ductility, especially when the density of twins is high and the size of twins is at the nanoscale. On one hand, TBs can block dislocation sliding and dislocations can be piled-up at TBs for improving strength in materials. Upon further plastic deformation, twins may be transformed into NGs via shear banding or high-angle GBs by dislocations accumulation [66]. On the other hand, TB could nucleate and emit dislocations during plastic deformation when the stress concentration at TBs is high enough. Atomistic and MD simulations have also shown that TBs can assist dislocation generation [67]. The main factors affecting the strengthening of TBs are the spacing of TBs and the volume fraction of twins. In recent years, numerical research indicated that when the spacing of TBs decreases to nanoscale, the strengthening effect is particularly remarkable, and the other mechanical properties in metals, such as ductility, strain rate sensitivity, wear resistance, fatigue performance, fracture toughness, can also be significantly improved [68–73].

4.1. Strength and Ductility

Strength and ductility are the important mechanical properties of metals and alloys, but there exists a trade-off dilemma between them, limiting the potential use of many structural metals and alloys. Numerical research have proven that the strength can be effectively elevated in metals and alloys without much sacrifice of ductility [74–76]. Especially in copper, the strength of NT Cu can reach impressive gigapascal scale, over more than fifteen times of its CG counterpart [75]. The electro-deposited Cu sample with high density of nanoscale growth twins showed that the strength and ductility can increase simultaneously with decreasing TB spacing when the mean grain size keeps constant [74–77] (Figures 12a and 13). The strengthening effect of TBs is analogous to that of conventional GBs.

The in-situ transmission electron microscope (TEM) and other postmortem TEM investigations showed that TBs are strong barriers to dislocations, and glissile partial dislocations can be generated at TBs for accommodating plastic deformation, which releases the local stress concentration and promotes further plastic deformation [66,78–80]. Another approach to introduce nanotwins in metals and alloys was severe plastic deformation (SPD) technique, which can generate grain refinement and deformation twinning. For materials with low SFE, such as Cu-Zn [80,81], Cu-Al [82,83], FeCoCrNiMn [84,85], CoCrNi [17,86,87], and other high/medium entropy alloys (H/MEAs), twinning is easier to occur than slipping, especially at the low temperature [88] and high strain rate [89]. Nanostructured Cu sample by means of dynamic plastic deformation (DPD) at liquid nitrogen temperature and subsequent short-time annealing showed surprisingly good strength–ductility combination [90]. The annealed structure as a typical heterogeneous structure, containing nano-grains with nanotwins and static recrystallized grains, showed excellent performance in work hardening ability. The similar heterogeneous structures also work effectively in Cu-Zn and Cu-Al alloys, as shown in Figure 12c,d [80,91]. High manganese TWIP steels are perfect candidates in crash safety of automobile due to their excellent work hardening capability, but the TWIP steels with CG structure usually have low yielding strength [92]. A gradient NT structure [47] was generated by applying torsion to double the yielding strength without reduction of ductility in a TWIP steel. In addition, multiple twins can promote plastic deformation in metals and alloys, while higher order twins are difficult to form in the metals and alloys with high SFE [94,95]. Five-order twins were fabricated in pure silver (Ag) with extremely low SFE by SMAT and uniaxial pre-loading [96]. The Ag with multiple twins can improve its strength by over three times without sacrificing ductility when compared to the CG counterpart. The hierarchical NT structures in FCC metals have been proposed to be a novel structure to bring out higher strength/ductility than NT counterparts due to their unique deformation phenomena [97].
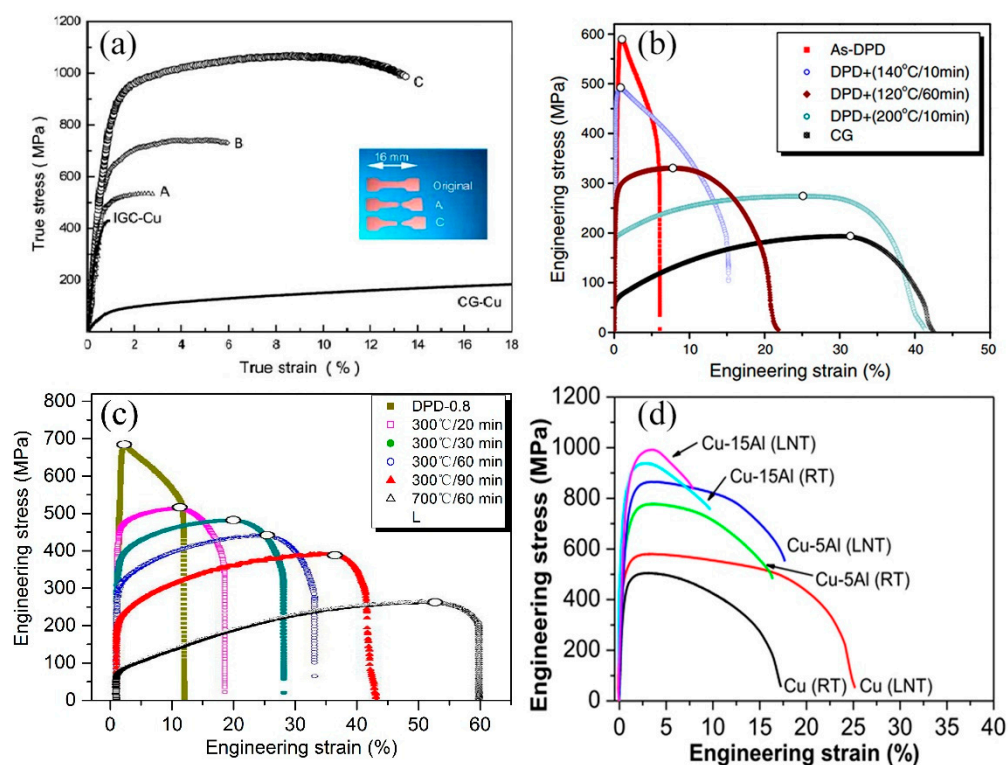

Figure 12. Typical tensile strain-stress curves. (**a**) as deposited Cu (adapted from Refs. [75]); (**b**) DPD-Cu (adapted from Refs. [90]); (**c**) DPD-Cu-Zn (adapted from Refs. [80]); (**d**) Cu-Al (adapted from [91]).
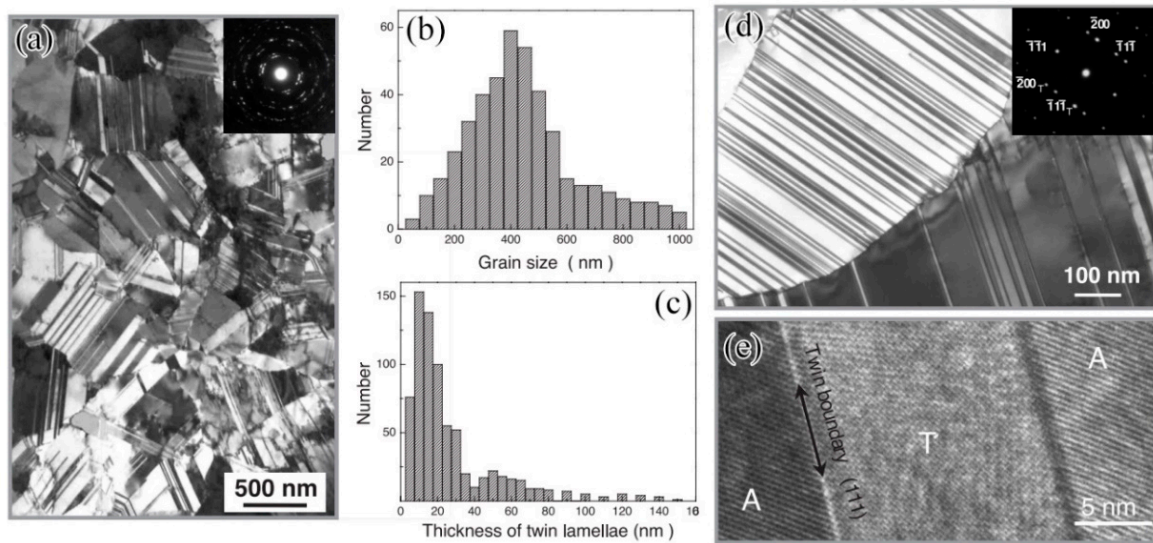
Figure 13. TEM observations of the typical microstructure in an as-deposited NT-Cu sample. Bright-field TEM image (**a**) and the electron diffraction pattern (inset) show roughly equiaxed submicrometer-sized grains with random orientations separated by high-angle GBs. The statistical distributions for grain size (**b**) and for thickness of the twin/matrix lamellae (**c**) (obtained from the many TEM images of the same sample). Electron diffraction patterns (inset in (**d**)) indicate that the twins in each grain are parallel to each other in {111} planes (**d**), and high-resolution TEM images (**e**) show that the twins follow a sequence of ATATA, with twinning elements, for example, A: $(\bar{1}1\bar{1})/[\bar{1}12]$ and T: $(\bar{1}11)/[1\bar{1}2]$. Adapted from [74].

4.2. Strain Rate Effect and Activation Volume

Mechanical performance of metals and alloys is always sensitive to strain rates, especially for NC metals [98–103]. The SRS can be defined as: $m = \partial ln\sigma / \partial ln\dot{\varepsilon}$, where σ is the flow stress and $\dot{\varepsilon}$ is the strain rate. SRS generally reflects the ability of materials to resist localized deformation when deformation is unstable at higher strain rate [71,98–103]. In general, the high SRS means higher elevation in flow stress with increasing strain rate. Enhancing SRS could prevent early onset of necking and nonuniform plastic deformation at a higher strain rate. TBs, which serve as a special kind of boundaries with low energy, can obstruct dislocation motion for providing higher strength and larger SRS. Activation volume of plastic deformation reflects the mechanism of rate-controlling deformation. The activation volume of NT-Cu was measured to be about dozens of b^3 (here, b is the Burgers vector of Cu, $b = 0.265$ nm), much lower than that for UFG-Cu without twins (several hundred of b^3), in which the main rate-controlling deformation mechanism might be forest dislocation interaction. Tensile strain rate jump tests [99] and different strain rate tensile tests [71] have revealed that NT-Cu with higher density of nanotwins can have a higher elevation of flow stress with increasing strain rate. The flow stress for the samples of NT-Cu with a mean TB spacing of 15 nm (referred to NT-Cu-fine) can be elevated more than 150 MPa when the strain rate increases from 10^{-5} to 10^{-2} s^{-1}. However, the corresponding elevation value for the samples of NT-Cu with a mean TB spacing of 100 nm (referred to NT-Cu-coarse) is only about 50 MPa. In addition, the average grain size for both NT-Cu-Fine and NT-Cu-Coarse samples is similar (about 400–500 nm), excluding the grain size effect. The TEM observations of NT-Cu-fine samples after deformation showed that TBs are curved comparing to the straight TBs before test and high-density dislocations are observed to pile up along TBs. Stress-relaxation tests are standard methods to measure strain hardening rate, SRS, activation volume and mobile dislocation density. The TB spacing always has significant influences on the NT Cu's mechanical performance [104]. The NT-Cu with high density of twins show a much lower exhaustion rate of mobile dislocations as the applied stress increases, when compared to NC Cu without twins [105]. These results suggest that TBs can preserve mobile dislocations more effectively. MD simulations have indicated that dislocations may propagate into

the adjacent part of twins by cutting through TBs when dislocations interact with Σ3 coherent TBs in NT-Cu [99], which would contribute to sufficient strain hardening by the mobile dislocations at the coherent TBs.

4.3. Fatigue and Damage Tolerance

Fatigue behaviors of materials refer to the mechanical properties subjected to cyclic loading [70]. In applications, more than ninety percent of the metal components or structures fail due to fatigue loading, which is normally tension-tension or tension-compression cyclic loading. The corresponding theories and experiments have been proposed and studied for homogeneous materials, such as the Griffith fracture theory, the J-integral and the Paris's low. However, the fatigue and fracture deformation mechanisms of the materials with heterogeneous structures are still far from well understood [106–110]. Pan et al. reported a history-independent and stable cyclic response in highly-oriented NT-Cu samples [70]. They defined the so-called "necklace" dislocations, which carry plastic deformation strongly correlating across multiple TBs. The corresponding simulations indicated that the "necklace" dislocations move collectively back and forth along the TBs under cycle loading, so there was no damage accumulation by the cyclic stresses in the samples. The coherent TBs usually are generated in materials as an ideal toughening "phase" to prevent stress concentration and improve fracture resistance. The in situ TEM observations [106] and MD simulations [107–110] revealed that a zigzag crack path was remained in the thin foil of NT Cu during fracture process due to the dislocation pile up against TBs and across TBs, as shown in Figure 14. The detailed analysis of MD results revealed that the mechanism of fracture involves the dislocation-mediated local thinning ahead of the crack tip instead of cleavage fracture. On one hand, the zigzag mode of crack path would cause more energy dissipation compared to a straight crack path. On the other hand, there was also small section of crack along coherent TBs which have higher fracture resistances than incoherent GBs. Therefore, TBs could increase the fracture resistances effectively [111–122]. Xiong et al. have indicated that 316L stainless steels with bundles of nanoscale deformation twins have beneficial to enhance the fracture resistance [113,114]. The results showed that the twinning bundles constrict void initiation in nano-grain matrix, coincidently resist crack propagation by acting as crack bridging ligaments.
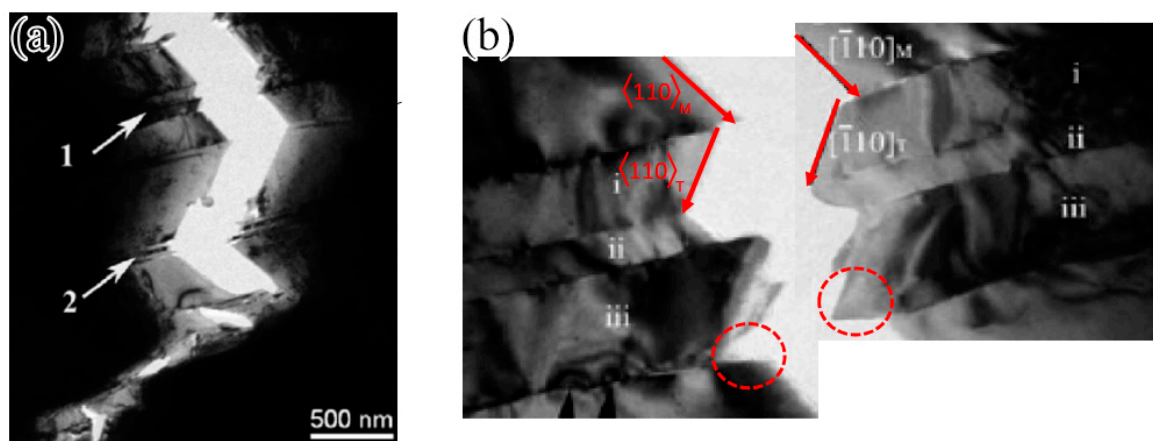

Figure 14. In situ TEM images of crack growth process in a thin foil of NT Cu. (**a**) A zigzag crack formed during tensile loading. (**b**) Magnified images of region 1 in (**a**), circles indicate the short crack edges on TBs. Adapted from [107].

The desirable mechanical properties, such as high strength, high ductility, high SRS, high damage tolerance, can be obtained in materials with nanotwins [66,115]. The enormous chanllenges fall in the processing of higher density of nanotwins, especially for materials with high SFE. This deserves futher deep investigations in the future.

5. Nanoprecipitate

Precipitation strengthening is a common approach to enhance the strength of materials. However, the particles in large size usually cause stress concentration due to deformation incompatibility, leading to microvoids, microcracks and even earlier fractures. Nanoprecipitate can solve this dilemma and obtain both high strength and large ductility in metals and alloys.

Liu et al. fabricated the La_2O_3 nanoparticles in the nanostructured molybdenum (Mo) alloys, which exhibit an unprecedented combination of strength and ductility [116]. The intragranular La_2O_3 nanoparticles could generate and store dislocations, prolonging ductility with high strength in nanostructured Mo alloys. The particles also play an efficient role as barriers to dislocation slipping. The TEM images showed that the dislocations are pinned by nanoparticles and generated around the nanoparticles. The spatial distribution and density of the nanoprecipitates also influence work-hardening ability. By aging treatment, nanoprecipitates with rich content of Ni, Ti and Al were dispersed in medium-Mn alloys [117]. The strength and the uniform elongation were both elevated effectively due to the nanoprecipitates [117]. The intragranular precipitates promote ductility in martensite by accumulating dislocations. Precipitation strengthening is also considered to be an effective strengthening mechanism in HEAs. Fu et al. designed and fabricated an $Fe_{25}Co_{25}Ni_{25}Al_{10}Ti_{15}$ dual-phase HEA that contains an FCC matrix (γ) with a small volume fraction of body-centered cubic (BCC) phase [118]. There are some primary nanoprecipitates γ' and secondary nanoprecipitates γ^* in FCC matrix. Based on the observation of in situ compression tests in the TEM, dislocation slipping was observed to be impeded by shearing both the primary precipitates γ' and the secondary precipitates γ^*. Thus, the HEA with high density of hierarchical intragranular nanoprecipitates shows an unprecedented tensile yield strength, which is ~1860 MPa.

We [119] developed an electroplating protocol in pure Ni to deploy NGs inside large grains: so-called nanodomained Ni (Figure 15c). These nanodomains can block dislocations and leave ample room for dislocation to entangle and store in the large grains, resulting in simultaneous high strength and large ductility and evading the strength–ductility trade-off. The conventional nanostructured Ni has a higher strength, but the uniform elongation decreases drastically with decreasing grain size, as shown in the curves of A, B and C in Figure 15a. Figure 15b summarizes the typical "banana curve" (trade-off) for the Ni and Cu with homogeneous structure (the blue region) by normalized yield strength and normalized uniform tensile elongation (ductility). Outside of the blue region, the green dashed line shows the data with an outstanding combination of strength and ductility for Cu and other steels with heterogeneous structures. The nanodomained Ni stands out as an exception with its NG-level strength and CG-like ductility. And the tensile stress–strain curve of the nanodomained Ni (Figure 15a, curve F) shows the higher work hardening rate than that of the Ni with other structures, which is the reason for such a large uniform elongation. High resolution post-mortem TEM observations of indicate much higher dislocation density near the boundaries of the domains (Figure 15d). The MD simulations have also confirmed this phenomenon [120].
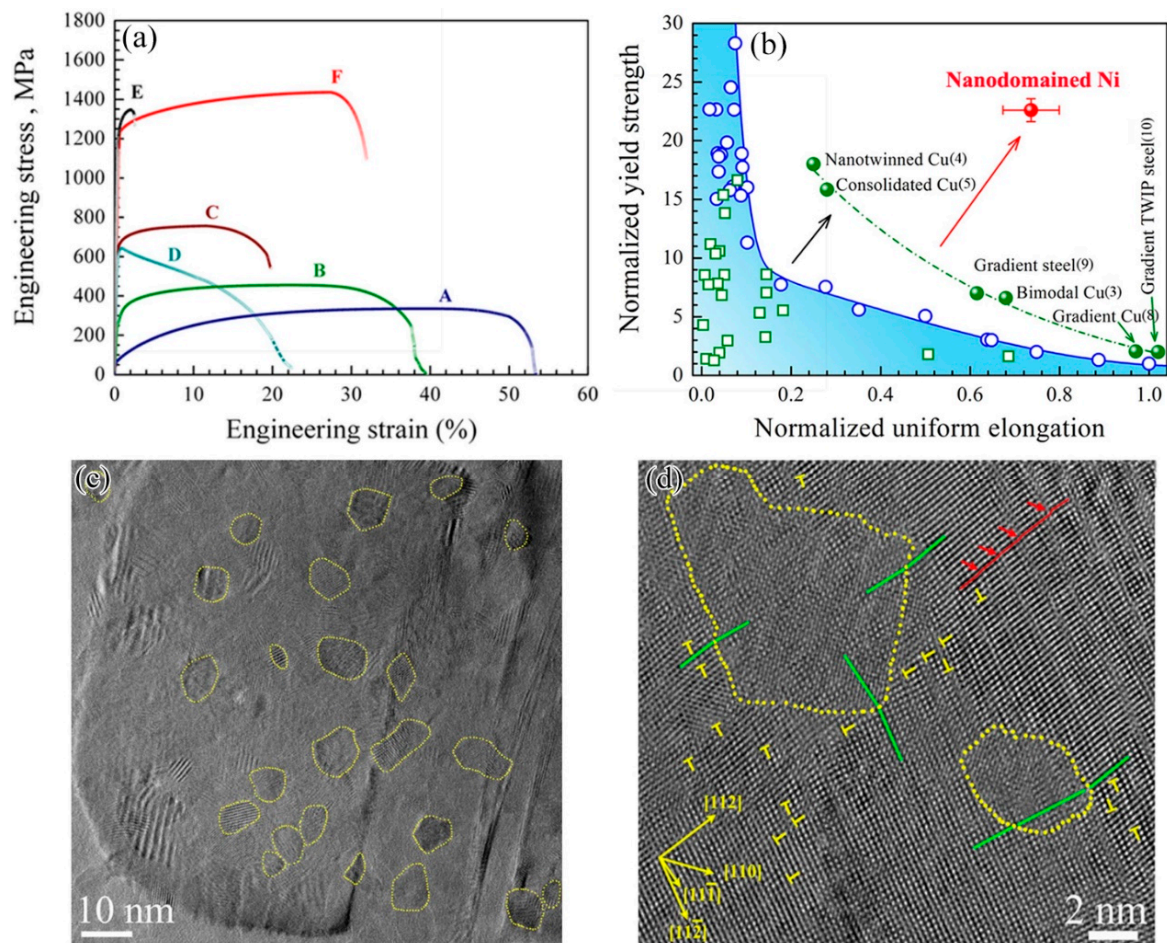
Figure 15. (**a**) Engineering tensile stress–strain curves at a strain rate of 4×10^{-4} s^{-1}: Curve A: as-annealed CG Ni with an average grain size of 27 μm; Curve B: electrodeposited (ED) Ni (d = 1μm); Curve C: electrodeposited UFG Ni (d = 200 nm); Curve D: UFG Ni obtained via equal channel angular pressing (ECAP) for one pass; Curve E: ED nanocrystalline Ni (d = 18 nm); Curve F: electroplated nanodomained Ni (d = 150 nm, d_{domain} = 7 nm). (**b**) Normalized yield strength versus normalized tensile uniform elongation for metals. (**c**) TEM images of nanodomained Ni, showing low-angle domain boundaries (LADBs). (**d**) High-resolution electron microscope (HREM) images showing the dislocation pile-ups. (adapted from [119]).

As shown in Figure 16, moving dislocations are observed to be blocked and pinned by the domain boundaries. Although the average domain diameter is as small as about 7 nm and the volume fraction is around 2.4%, these domains appear to be stable upon tensile deformation. Such heterogeneously architected nanostructure has been proven to be a valuable strategy to evade the strength–ductility trade-off in pure metals [117–120].
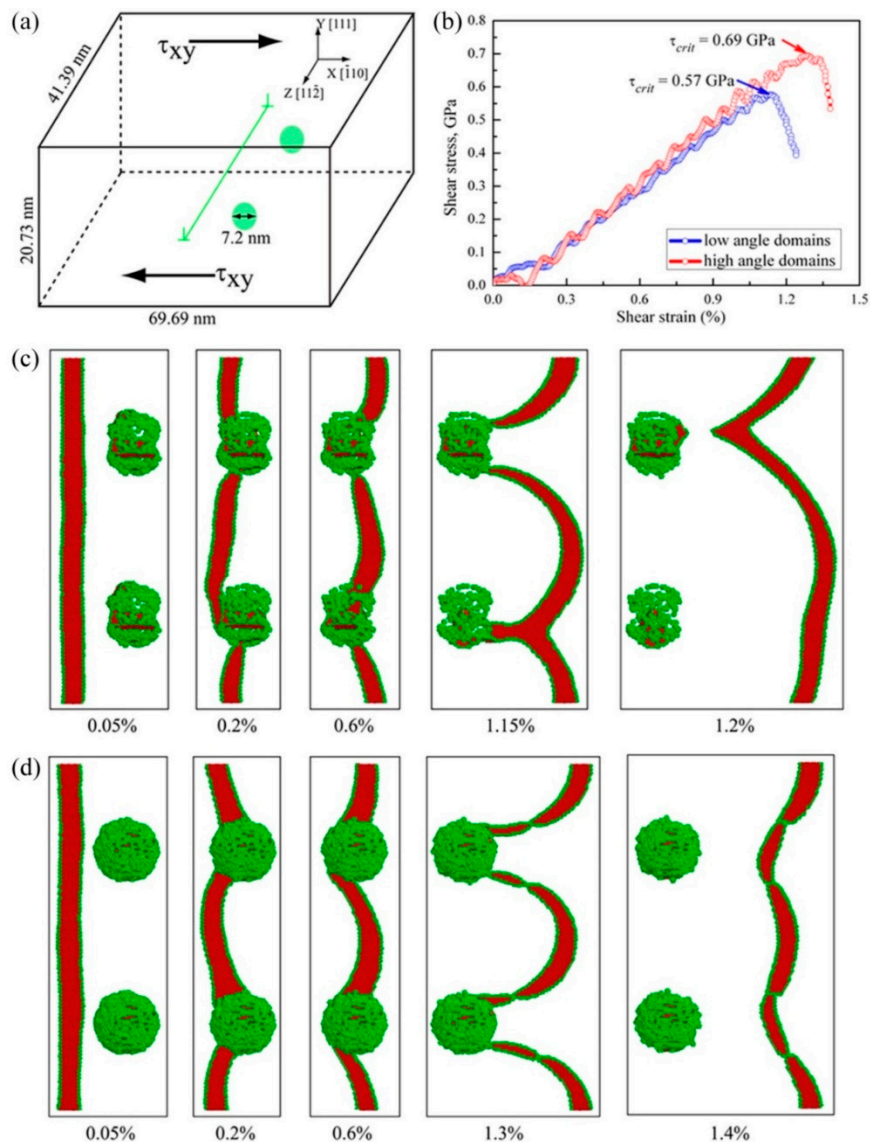
Figure 16. MD simulations of slip-nanodomain interactions. (**a**) Configuration for simulation cell with a straight edge dislocation and two nanodomains. (**b**) Simulated shear stress-shear strain curves as the straight dislocation is blocked by the nanodomains. (**c**) A sequence of snapshots at varying shear strains showing the pinning of the dislocation and its subsequent bowing around the nanodomains with LADB. (**d**) A sequence of snapshots at varying shear strains showing the pinning of the dislocation and its subsequent bowing around the nanodomains with high-angle domain boundaries (HADB). Adapted from [119].

6. Conclusions, Future Perspective and Challenges

In this paper, the plastic behaviors and the corresponding deformation physics for heterogeneous grain/lamellar/phase structures, gradient structure, NT structure and structure with nanoprecipitates have been reviewed. The design concept for these heterogeneous structures is to delocalize strain concentration for improving ductility through extra hardening effects. These heterogeneous structures have can increase opportunities for dislocation storage by GNDs over the homogeneous counterparts. These GNDs are generated by the strain gradients and the plastic deformation incompatibility between different domains with dramatically varying mechanical properties. Thus, unexpected high uniform elongation can be achieved for high strength metals and alloys, evading the strength–ductility trade

off. These deformation mechanisms and deformation physics are applicable not only to the uniaxial loading condition but also to the dynamic and fatigue conditions.

In one hand, one may think to raise the microstructure inhomogeneity to achieve stronger strain gradients and better extra strain hardening, on the other hand the interfaces with too large microstructure inhomogeneity might not be strong enough to accommodate the high strain gradients and the high density of GNDs, resulting in a quick failure at the interfaces and a lower ductility. The size and spacing of the domains are also critical for optimizing the mechanical properties of heterogeneous structures. Smaller domains can generate more interfaces, resulting in more spaces for a higher density of GNDs and better ductility. However, too-small domains may cause the overlapping of GNDs distributions between neighboring domains, resulting in decreasing ductility. Thus, how to control the microstructure heterogeneity to obtain optimizing mechanical properties remains an unresolved issue and needs extensive experimental and theoretical efforts in the future. Moreover, manufacturing the desired microstructure with predesigned heterogeneity is a great challenge. Previous studies on the dynamic behaviors of heterogeneous structures were conducted in an "in-situ" manner; however, "in-situ" dynamic experiments with accurate measurements of temperature rise history and strain field history must be developed to better understand these dynamic processes. Experimental evidence for the fatigue behaviors of heterogeneous structures are also limited, and more research should be conducted to obtain a comprehensive understanding on fatigue mechanisms (including fatigue crack growth behaviors, cyclic softening/strengthening behaviors) in the future. Moreover, additional efforts should focus on the fracture toughness, impact toughness, superplastic behaviors and thermal stability of the heterogeneous structures.

Author Contributions: Conceptualization, F.Y. and X.W.; methodology, F.Y.; validation, F.Y. and X.W.; writing—Sections 1, 3 and 6, F.Y., writing—Section 2, M.Y. writing—Sections 4 and 5, Y.M.; visualization, F.Y., M.Y. and Y.M.; supervision, F.Y.; project administration, F.Y. and X.W.; funding acquisition, F.Y, M.Y., and X.W.

References

1. Meyers, M.A.; Mishra, A.; Benson, D.J. Mechanical properties of nanocrystalline materials. *Prog. Mater. Sci.* **2006**, *51*, 427–556. [CrossRef]
2. Ma, E.; Zhu, T. Towards strength–ductility synergy through the design of heterogeneous nanostructures in metals. *Mater. Today* **2017**, *20*, 323–331. [CrossRef]
3. Wu, X.L.; Zhu, Y.T. Heterogeneous materials: A new class of materials with unprecedented mechanical properties. *Mater. Res. Lett* **2017**, *5*, 527–532. [CrossRef]
4. Ovid'ko, I.A.; Valiev, R.Z.; Zhu, Y.T. Review on superior strength and enhanced ductility of metallic nanomaterials. *Prog. Mater. Sci.* **2018**, *94*, 462–540. [CrossRef]
5. Valiev, R.Z.; Estrin, Y.; Horita, Z.; Langdon, T.G.; Zehetbauer, M.J.; Zhu, Y.T. Fundamentals of superior properties in bulk NanoSPD materials. *Mater. Res. Lett* **2016**, *4*, 1–21. [CrossRef]
6. Cao, Y.; Ni, S.; Liao, X.Z.; Song, M.; Zhu, Y.T. Structural evolutions of metallic materials processed by severe plastic deformation. *Mater. Sci. Eng. R.* **2018**, *133*, 1–59. [CrossRef]
7. Valiev, R.Z.; Islamgaliev, R.K.; Alexandrov, I.V. Bulk nanostructured materials from severe plastic deformation. *Prog. Mater. Sci.* **2000**, *45*, 103–189. [CrossRef]
8. Valiev, R.Z.; Alexandrov, I.V.; Zhu, Y.T.; Lowe, T.C. Paradox of strength and ductility in metals processed by severe plastic deformation. *J. Mater. Res.* **2002**, *17*, 5–8. [CrossRef]
9. Valiev, R. Nanostructuring of metals by severe plastic deformation for advanced properties. *Nat. Mater.* **2004**, *3*, 511–516. [CrossRef]

10. Langdon, T.G. Twenty-five years of ultrafine-grained materials: Achieving exceptional properties through grain refinement. *Acta Mater.* **2013**, *61*, 7035–7059. [CrossRef]

11. Lu, K. Making strong nanomaterials ductile with gradients. *Science* **2014**, *345*, 1455–1456. [CrossRef] [PubMed]

12. Lu, K. Stabilizing nanostructures in metals using grain and twin boundary architectures. *Nat. Rev. Mater.* **2016**, *1*, 13. [CrossRef]

13. Cheng, Z.; Zhou, H.F.; Lu, Q.H.; Gao, H.J.; Lu, L. Extra strengthening and work hardening in gradient nanotwinned metals. *Science* **2018**, *362*, 559–567. [CrossRef]

14. Wu, X.L.; Jiang, P.; Chen, L.; Yuan, F.P.; Zhu, Y.T. Extraordinary strain hardening by gradient structure. *Proc. Natl. Acad. Sci. USA* **2014**, *111*, 7197–7201. [CrossRef]

15. Wu, X.L.; Jiang, P.; Chen, L.; Zhang, J.F.; Yuan, F.P.; Zhu, Y.T. Synergetic Strengthening by Gradient Structure. *Mater. Res. Lett.* **2014**, *2*, 185–191. [CrossRef]

16. Wu, X.L.; Yang, M.X.; Yuan, F.P.; Wu, G.L.; Wei, Y.J.; Huang, X.X.; Zhu, Y.T. Heterogeneous lamella structure unites ultrafine-grain strength with coarse-grain ductility. *Proc. Natl. Acad. Sci. USA* **2015**, *112*, 14501–14505. [CrossRef]

17. Yang, M.X.; Yan, D.S.; Yuan, F.P.; Jiang, P.; Ma, E.; Wu, X.L. Dynamically reinforced heterogeneous grain structure prolongs ductility in a medium-entropy alloy with gigapascal yield strength. *Proc. Natl. Acad. Sci. USA* **2018**, *115*, 7224–7229. [CrossRef] [PubMed]

18. Wang, Y.M.; Chen, M.W.; Zhou, F.H.; Ma, E. High tensile ductility in a nanostructured metal. *Nature* **2002**, *419*, 912–915. [CrossRef] [PubMed]

19. Shukla, S.; Choudhuri, D.; Wang, T.; Liu, K.; Wheeler, R.; Williams, S.; Gwalani, B.; Mishra, R.S. Hierarchical features infused heterogeneous grain structure for extraordinary strength–ductility synergy. *Mater. Res. Lett.* **2018**, *6*, 676–682. [CrossRef]

20. Wu, G.; Chan, K.C.; Zhu, L.L.; Sun, L.G.; Lu, J. Dual-phase nanostructuring as a route to high-strength magnesium alloys. *Nature* **2017**, *545*, 80–83. [CrossRef]

21. Shi, P.J.; Ren, W.L.; Zheng, T.X.; Ren, Z.M.; Hou, X.L.; Peng, J.C.; Hu, P.F.; Gao, Y.F.; Zhong, Y.B.; Liaw, P.K. Enhanced strength–ductility synergy in ultrafine-grained eutectic high-entropy alloys by inheriting microstructural lamellae. *Nat. Commun.* **2019**, *10*, 489. [CrossRef] [PubMed]

22. Koyama, M.; Zhang, Z.; Wang, M.M.; Ponge, D.; Raabe, D.; Tsuzaki, K.; Noguchi, H.; Tasan, C.C. Bone-like crack resistance in hierarchical metastable nanolaminate steels. *Science* **2017**, *355*, 1055–1057. [CrossRef] [PubMed]

23. He, B.B.; Hu, B.; Yen, H.W.; Cheng, G.J.; Wang, Z.K.; Luo, H.W.; Huang, M.X. High dislocation density-induced large ductility in deformed and partitioned steels. *Science* **2017**, *357*, 1029–1032. [CrossRef]

24. Liang, Y.J.; Wang, L.J.; Wen, Y.R.; Cheng, B.Y.; Wu, Q.L.; Cao, T.Q.; Xiao, Q.; Xue, Y.F.; Sha, G.; Wang, Y.D.; et al. High-content ductile coherent nanoprecipitates achieve ultrastrong high-entropy alloys. *Nat. Commun.* **2018**, *9*, 4063. [CrossRef] [PubMed]

25. Huang, C.X.; Wang, Y.F.; Ma, X.L.; Yin, S.; Hoeppel, H.W.; Goeken, M.; Wu, X.L.; Gao, H.J.; Zhu, Y.T. Interface affected zone for optimal strength and ductility in heterogeneous laminate. *Mater. Today* **2018**, *21*, 713–719. [CrossRef]

26. Ma, Y.; Yuan, F.P.; Yang, M.X.; Jiang, P.; Ma, E.; Wu, X.L. Dynamic shear deformation of a CrCoNi medium-entropy alloy with heterogeneous grain structures. *Acta Mater.* **2018**, *148*, 407–418. [CrossRef]

27. Wu, X.L.; Yang, M.X.; Yuan, F.P.; Chen, L.; Zhu, Y.T. Combining gradient structure and TRIP effect to produce austenite stainless steel with high strength and ductility. *Acta Mater.* **2016**, *112*, 337–346. [CrossRef]

28. Yang, M.X.; Yuan, F.P.; Xie, Q.G.; Wang, Y.D.; Ma, E.; Wu, X.L. Strain hardening in Fe-16Mn-10Al-0.86C-5Ni high specific strength steel. *Acta Mater.* **2016**, *109*, 213–222. [CrossRef]

29. Ma, Y.; Yang, M.X.; Jiang, P.; Yuan, F.P.; Wu, X.L. Plastic deformation mechanisms in a severely deformed Fe-Ni-Al-C alloy with superior tensile properties. *Sci. Rep.* **2017**, *7*, 15619. [CrossRef]

30. Miserez, A.; Schneberk, T.; Sun, C.; Zok, F.W.; Waite, J.H. The transition from stiff to compliant materials in squid beaks. *Science* **2008**, *319*, 1816–1819. [CrossRef]

31. Gao, S.L.; Maeder, E.; Plonka, R. Nanostructured-coatings of glass fibers: Improvement of alkali resistance and mechanical properties. *Acta Mater.* **2007**, *55*, 1043–1052. [CrossRef]

32. Edalati, K.; Matsuda, J.; Iwaoka, H.; Toh, S.; Akiba, E.; Horita, Z. High-pressure torsion of TiFe intermetallics for activation of hydrogen storage at room temperature with heterogeneous nanostructure. *Int. J. Hydrog. Energy* **2013**, *38*, 4622–4627. [CrossRef]

33. Liu, R.; Duay, J.; Lee, S.B. Heterogeneous nanostructured electrode materials for electrochemical energy storage. *Chem. Commun.* **2011**, *47*, 1384–1404. [CrossRef]

34. Tong, W.P.; Han, Z.; Wang, L.M.; Lu, J.; Lu, K. Low-temperature nitriding of 38CrMoAl steel with a nanostructured surface layer induced by surface mechanical attrition treatment. *Surf. Coat. Tech.* **2008**, *202*, 4957–4963. [CrossRef]

35. Lu, K.; Lu, J. Surface nanocrystallization (SNC) of metallic materials-presentation of the concept behind a new approach. *J. Mater. Sci. Technol.* **1999**, *15*, 193–197.

36. Suresh, S. Graded materials for resistance to contact deformation and damage. *Science* **2001**, *292*, 2447–2451. [CrossRef] [PubMed]

37. Yuan, F.P.; Jiang, P.; Xie, J.J.; Wu, X.L. Analysis of spherical indentation of materials with plastically graded surface layer. *Int. J. Solids. Struct.* **2012**, *49*, 527–536. [CrossRef]

38. Tong, W.P.; Tao, N.R.; Wang, Z.B.; Lu, J.; Lu, K. Nitriding iron at lower temperatures. *Science* **2003**, *299*, 686–688. [CrossRef] [PubMed]

39. Roland, T.; Retraint, D.; Lu, K.; Lu, J. Fatigue life improvement through surface nanostructuring of stainless steel by means of surface mechanical attrition treatment. *Scr. Mater.* **2006**, *54*, 1949–1954. [CrossRef]

40. Chen, A.Y.; Li, D.F.; Zhang, J.B.; Song, H.W.; Lu, J. Make nanostructured metal exceptionally tough by introducing non-localized fracture behaviors. *Scr. Mater.* **2008**, *59*, 579–582. [CrossRef]

41. Li, W.L.; Tao, N.R.; Lu, K. Fabrication of a gradient nano-micro-structured surface layer on bulk copper by means of a surface mechanical grinding treatment. *Scr. Mater.* **2008**, *59*, 546–549. [CrossRef]

42. Fang, T.H.; Li, W.L.; Tao, N.R.; Lu, K. Revealing Extraordinary Intrinsic Tensile Plasticity in Gradient Nano-Grained Copper. *Science* **2011**, *331*, 1587–1590. [CrossRef]

43. Jerusalem, A.; Dickson, W.; Perez-Martin, M.J.; Dao, M.; Lu, J.; Galvez, F. Grain size gradient length scale in ballistic properties optimization of functionally graded nanocrystalline steel plates. *Scr. Mater.* **2013**, *69*, 773–776. [CrossRef]

44. Liu, X.C.; Zhang, H.W.; Lu, K. Strain-Induced Ultrahard and Ultrastable Nanolaminated Structure in Nickel. *Science* **2013**, *342*, 337–340. [CrossRef]

45. Huang, H.W.; Wang, Z.B.; Yong, X.P.; Lu, K. Enhancing torsion fatigue behaviour of a martensitic stainless steel by generating gradient nanograined layer via surface mechanical grinding treatment. *Mater. Sci. Technol.* **2013**, *29*, 1200–1205. [CrossRef]

46. Fang, T.H.; Tao, N.R.; Lu, K. Tension-induced softening and hardening in gradient nanograined surface layer in copper. *Scr. Mater.* **2014**, *77*, 17–20. [CrossRef]

47. Wei, Y.J.; Li, Y.Q.; Zhu, L.C.; Liu, Y.; Lei, X.Q.; Wang, G.; Wu, Y.X.; Mi, Z.L.; Liu, J.B.; Wang, H.T.; et al. Evading the strength- ductility trade-off dilemma in steel through gradient hierarchical nanotwins. *Nat. Commun.* **2014**, *5*, 3580. [CrossRef] [PubMed]

48. Li, J.J.; Chen, S.H.; Wu, X.L.; Soh, A.K. A physical model revealing strong strain hardening in nano-grained metals induced by grain size gradient structure. *Mater. Sci. Eng. A* **2015**, *620*, 16–21. [CrossRef]

49. Huang, H.W.; Wang, Z.B.; Lu, J.; Lu, K. Fatigue behaviors of AISI 316L stainless steel with a gradient nanostructured surface layer. *Acta Mater.* **2015**, *87*, 150–160. [CrossRef]

50. Li, W.B.; Yuan, F.P.; Wu, X.L. Atomistic tensile deformation mechanisms of Fe with gradient nano-grained structure. *AIP Adv.* **2015**, *5*, 087120. [CrossRef]

51. Ma, Z.W.; Liu, J.B.; Wang, G.; Wang, H.T.; Wei, Y.J.; Gao, H.J. Strength gradient enhances fatigue resistance of steels. *Sci. Rep.* **2016**, *6*, 22156. [CrossRef]

52. Yuan, F.P.; Chen, P.; Feng, Y.P.; Jiang, P.; Wu, X.L. Strain hardening behaviors and strain rate sensitivity of gradient-grained Fe under compression over a wide range of strain rates. *Mech. Mater.* **2016**, *95*, 71–82. [CrossRef]

53. Yang, M.X.; Pan, Y.; Yuan, F.P.; Zhu, Y.T.; Wu, X.L. Back stress strengthening and strain hardening in gradient structure. *Mater. Res. Lett.* **2016**, *4*, 145–151. [CrossRef]

54. Li, J.J.; Weng, G.J.; Chen, S.H.; Wu, X.L. On strain hardening mechanism in gradient nanostructures. *Int. J. Plast.* **2017**, *88*, 89–107. [CrossRef]

55. Zhu, L.L.; Wen, C.S.; Gao, C.Y.; Guo, X.; Lu, J. A study of dynamic plasticity in austenite stainless steels with a gradient distribution of nanoscale twins. *Scr. Mater.* **2017**, *133*, 49–53. [CrossRef]

56. Wang, Y.; Yang, G.X.; Wang, W.J.; Wang, X.; Li, Q.; Wei, Y.J. Optimal stress and deformation partition in gradient materials for better strength and tensile ductility: A numerical investigation. *Sci. Rep.* **2017**, *7*, 10954. [CrossRef] [PubMed]

57. Bian, X.D.; Yuan, F.P.; Wu, X.L.; Zhu, Y.T. The evolution of strain gradient and anisotropy in gradient-structured metal. *Metall. Mater. Trans. A* **2017**, *48A*, 3951–3960. [CrossRef]

58. Bian, X.D.; Yuan, F.P.; Zhu, Y.T.; Wu, X.L. Gradient structure produces superior dynamic shear properties. *Mater. Res. Lett.* **2017**, *5*, 501–507. [CrossRef]

59. Chen, L.; Yuan, F.P.; Jiang, P.; Xie, J.J.; Wu, X.L. Mechanical properties and deformation mechanism of Mg-Al-Zn alloy with gradient microstructure in grain size and orientation. *Mater. Sci. Eng. A* **2017**, *694*, 98–109. [CrossRef]

60. Lin, Y.; Pan, J.; Zhou, H.F.; Gao, H.J.; Li, Y. Mechanical properties and optimal grain size distribution profile of gradient grained nickel. *Acta Mater.* **2018**, *153*, 279–289. [CrossRef]

61. Long, J.Z.; Pan, Q.S.; Tao, N.R.; Lu, L. Abnormal grain coarsening in cyclically deformed gradient nanograined Cu. *Scr. Mater.* **2018**, *145*, 99–103. [CrossRef]

62. Liu, X.L.; Yuan, F.P.; Zhu, Y.T.; Wu, X.L. Extraordinary Bauschinger effect in gradient structured copper. *Scr. Mater.* **2018**, *150*, 57–60. [CrossRef]

63. Yuan, F.P.; Yan, D.S.; Sun, J.D.; Zhou, L.L.; Zhu, Y.T.; Wu, X.L. Ductility by shear band delocalization in the nano-layer of gradient structure. *Mater. Res. Lett.* **2019**, *7*, 12–17. [CrossRef]

64. Lu, X.C.; Zhang, X.; Shi, M.X.; Roters, F.; Kang, G.Z.; Raabe, D. Dislocation mechanism based size-dependent crystal plasticity modeling and simulation of gradient nano-grained copper. *Int. J. Plast.* **2019**, *113*, 52–73. [CrossRef]

65. Zeng, Z.; Li, X.Y.; Xu, D.S.; Lu, L.; Gao, H.J.; Zhu, T. Gradient plasticity in gradient nano-grained metals. *Extreme Mech. Lett.* **2016**, *8*, 213–219. [CrossRef]

66. Lu, K.; Lu, L.; Suresh, S. Strengthening materials by engineering coherent internal boundaries at the nanoscale. *Science* **2009**, *324*, 349–352. [CrossRef] [PubMed]

67. Gu, P.; Dao, M.; Asaro, R.J.; Suresh, S. A unified mechanistic model for size-dependent deformation in nanocrystalline and nanotwinned metals. *Acta Mater.* **2011**, *59*, 6861–6868. [CrossRef]

68. Lu, L.; Schwaiger, R.; Shan, Z.W.; Dao, M.; Lu, K.; Suresh, S. Nano-sized twins induce high rate sensitivity of flow stress in pure copper. *Acta Mater.* **2005**, *53*, 2169–2179. [CrossRef]

69. Lu, L.; Chen, X.; Huang, X.; Lu, K. Revealing the maximum strength in nanotwinned copper. *Science* **2009**, *323*, 607–610. [CrossRef]

70. Pan, Q.S.; Zhou, H.F.; Lu, Q.H.; Gao, H.J.; Lu, L. History-independent cyclic response of nanotwinned metals. *Nature* **2017**, *551*, 214–217. [CrossRef]

71. Dao, M.; Lu, L.; Shen, Y.F.; Suresh, S. Strength, strain-rate sensitivity and ductility of copper with nanoscale twins. *Acta Mater.* **2006**, *54*, 5421–5432. [CrossRef]

72. Wei, Q.; Cheng, S.; Ramesh, K.T.; Ma, E. Effect of nanocrystalline and ultrafine grain sizes on the strain rate sensitivity and activation volume: fcc versus bcc metals. *Mater. Sci. Eng. A* **2004**, *381*, 71–79. [CrossRef]

73. Li, X.Y.; Wei, Y.J.; Lu, L.; Lu, K.; Gao, H.J. Dislocation nucleation governed softening and maximum strength in nanotwinned metals. *Nature* **2010**, *464*, 877–880. [CrossRef]

74. Lu, L.; Shen, Y.F.; Chen, X.H.; Qian, L.H.; Lu, K. Ultrahigh strength and high electrical conductivity in copper. *Science* **2004**, *304*, 422–426. [CrossRef]

75. Shen, Y.F.; Lu, L.; Lu, Q.H.; Jin, Z.H.; Lu, K. Tensile properties of copper with nano-scale twins. *Scr. Mater.* **2005**, *52*, 989–994. [CrossRef]

76. Sun, L.G.; He, X.Q.; Lu, J. Atomistic simulation study on twin orientation and spacing distribution effects on nanotwinned Cu films. *Philos. Mag.* **2015**, *95*, 3467–3485. [CrossRef]

77. Sun, L.G.; He, X.Q.; Lu, J. Nanotwinned and hierarchical nanotwinned metals: a review of experimental, computational and theoretical efforts. *npj Comput. Mater.* **2018**, *4*, 6. [CrossRef]

78. Zhang, X.; Wang, H.; Chen, X.H.; Lu, L.; Lu, K.; Hoagland, R.G.; Misra, A. High-strength sputter-deposited Cu foils with preferred orientation of nanoscale growth twins. *Appl. Phys. Lett.* **2006**, *88*, 173116. [CrossRef]

79. Wang, Y.B.; Wu, B.; Sui, M.L. Dynamical dislocation emission processes from twin boundaries. *Appl. Phys. Lett.* **2008**, *93*, 041906. [CrossRef]

80. Xiao, G.H.; Tao, N.R.; Lu, K. Strength–ductility combination of nanostructured Cu–Zn alloy with nanotwin bundles. *Scr. Mater.* **2011**, *65*, 119–122. [CrossRef]

81. Zhang, P.; Qu, S.; Yang, M.X.; Yang, G.; Wu, S.D.; Li, S.X.; Zhang, Z.F. Varying tensile fracture mechanisms of Cu and Cu–Zn alloys with reduced grain size: From necking to shearing instability. *Mater. Sci. Eng. A* **2014**, *594*, 309–320. [CrossRef]

82. Zhang, Y.; Tao, N.R.; Lu, K. Effects of stacking fault energy, strain rate and temperature on microstructure and strength of nanostructured Cu–Al alloys subjected to plastic deformation. *Acta Mater.* **2011**, *59*, 6048–6058. [CrossRef]

83. Qu, S.; An, X.H.; Yang, H.J.; Huang, C.X.; Yang, G.; Zang, Q.S.; Wang, Z.G.; Wu, S.D.; Zhang, Z.F. Microstructural evolution and mechanical properties of Cu–Al alloys subjected to equal channel angular pressing. *Acta Mater.* **2009**, *57*, 1586–1601. [CrossRef]

84. Laplanche, G.; Kostka, A.; Horst, O.M.; Eggeler, G.; George, E.P. Microstructure evolution and critical stress for twinning in the CrMnFeCoNi high-entropy alloy. *Acta Mater.* **2016**, *118*, 152–163. [CrossRef]

85. Gludovatz, B.; Hohenwarter, A.; Catoor, D.; Chang, E.H.; George, E.P.; Ritchie, R.O. A fracture-resistant high-entropy alloy for cryogenic applications. *Science* **2014**, *345*, 1153–1158. [CrossRef]

86. Yoshida, S.; Bhattacharjee, T.; Bai, Y.; Tsuji, N. Friction stress and Hall–Petch relationship in CoCrNi equi-atomic medium entropy alloy processed by severe plastic deformation and subsequent annealing. *Scr. Mater.* **2017**, *134*, 33–36. [CrossRef]

87. Slone, C.E.; Miao, J.; George, E.P.; Mills, M.J. Achieving ultra-high strength and ductility in equiatomic CrCoNi with partially recrystallized microstructures. *Acta Mater.* **2019**, *165*, 496–507. [CrossRef]

88. Miao, J.; Slone, C.E.; Smith, T.M.; Niu, C.; Bei, H.; Ghazisaeidi, M.; Pharr, G.M.; Mills, M.J. The evolution of the deformation substructure in a Ni-Co-Cr equiatomic solid solution alloy. *Acta Mater.* **2017**, *132*, 35–48. [CrossRef]

89. Li, Z.; Zhao, S.; Diao, H.; Liaw, P.K.; Meyers, M.A. High-velocity deformation of $Al_{0.3}CoCrFeNi$ high-entropy alloy: Remarkable resistance to shear failure. *Sci. Rep.* **2017**, *7*, 42742. [CrossRef]

90. Li, Y.S.; Zhang, Y.; Tao, N.R.; Lu, K. Effect of thermal annealing on mechanical properties of a nanostructured copper prepared by means of dynamic plastic deformation. *Scr. Mater.* **2008**, *59*, 475–478. [CrossRef]

91. Wei, K.X.; Horky, J.; Wei, W.; Zehetbauer, M.J.; Setman, D.; Schafler, E.; Hu, J. Enhancing tensile properties of Cu and Cu-Al alloys cryogenically processed by high pressure torsion. *J. Alloys Compd.* **2019**, *771*, 317–321. [CrossRef]

92. De Cooman, B.C.; Estrin, Y.; Kim, S.K. Twinning-induced plasticity (TWIP) steels. *Acta Mater.* **2018**, *142*, 283–362. [CrossRef]

93. Li, Y.S.; Zhang, Y.; Tao, N.R.; Lu, K. Effect of the Zener-Hollomon parameter on the microstructures and mechanical properties of Cu subjected to plastic deformation. *Acta Mater.* **2009**, *57*, 761–772. [CrossRef]

94. Yuan, F.P.; Wu, X.L. Formation sequences and roles of multiple deformation twins during the plastic deformation in nanocrystalline fcc metals. *Mater. Sci. Eng. A* **2013**, *580*, 58–65. [CrossRef]

95. Yuan, F.P.; Wu, X.L. Size effects of primary/secondary twins on the atomistic deformation mechanisms in hierarchically nanotwinned metals. *J. Appl. Phys.* **2013**, *113*, 203516. [CrossRef]

96. Liu, X.W.; Sun, L.G.; Zhu, L.L.; Liu, J.B.; Lu, K.; Lu, J. High-order hierarchical nanotwins with superior strength and ductility. *Acta Mater.* **2018**, *149*, 397–406. [CrossRef]

97. Wang, W.; Yuan, F.P.; Jiang, P.; Wu, X.L. Size effects of lamellar twins on the strength and deformation mechanisms of nanocrystalline hcp cobalt. *Sci. Rep.* **2017**, *7*, 9550. [CrossRef]

98. Wang, Y.; Hamza, A.; Ma, E. Temperature-dependent strain rate sensitivity and activation volume of nanocrystalline Ni. *Acta Mater.* **2006**, *54*, 2715–2726. [CrossRef]

99. Shen, Y.F.; Lu, L.; Dao, M.; Suresh, S. Strain rate sensitivity of Cu with nanoscale twins. *Scr. Mater.* **2006**, *55*, 319–322. [CrossRef]

100. Liang, Z.Y.; Wang, X.; Huang, W.; Huang, M.X. Strain rate sensitivity and evolution of dislocations and twins in a twinning-induced plasticity steel. *Acta Mater.* **2015**, *88*, 170–179. [CrossRef]

101. Yuan, F.P.; Wu, X.L. Shock response of nanotwinned copper from large-scale molecular dynamics simulations. *Phys. Rev. B* **2012**, *86*, 134108. [CrossRef]

102. You, Z.S.; Lu, L. Effect of strain rate on tensile ductility and fracture behavior of bulk nanotwinned copper. *Adv. Eng. Mater.* **2015**, *17*, 1754–1759. [CrossRef]

103. Yuan, F.P.; Chen, L.; Jiang, P.; Wu, X.L. Twin boundary spacing effects on shock response and spall behaviors of hierarchically nanotwinned fcc metals. *J. Appl. Phys.* **2014**, *115*, 063509. [CrossRef]

104. Lu, L.; Zhu, T.; Shen, Y.F.; Dao, M.; Lu, K.; Suresh, S. Stress relaxation and the structure size-dependence of plastic deformation in nanotwinned copper. *Acta Mater.* **2009**, *57*, 5165–5173. [CrossRef]

105. Schwaiger, R.; Moser, B.; Dao, M.; Chollacoop, N.; Suresh, S. Some critical experiments on the strain-rate sensitivity of nanocrystalline nickel. *Acta Mater.* **2003**, *51*, 5159–5172. [CrossRef]

106. Pan, Q.S.; Lu, Q.H.; Lu, L. Fatigue behavior of columnar-grained Cu with preferentially oriented nanoscale twins. *Acta Mater.* **2013**, *61*, 1383–1393. [CrossRef]

107. Zeng, Z.; Li, X.Y.; Lu, L.; Zhu, T. Fracture in a thin film of nanotwinned copper. *Acta Mater.* **2015**, *98*, 313–317. [CrossRef]

108. Sun, L.G.; He, X.Q.; Wang, J.B.; Lu, J. Deformation and failure mechanisms of nanotwinned copper films with a pre-existing crack. *Mater. Sci. Eng. A* **2014**, *606*, 334–345. [CrossRef]

109. Yuan, F.P.; Wu, X.L. Atomistic scale fracture behaviours in hierarchically nanotwinned metals. *Philos. Mag.* **2013**, *93*, 3248–3259. [CrossRef]

110. Yuan, F.P.; Wu, X.L. Size effect and atomistic deformation mechanisms of hierarchically nanotwinned fcc metals under nanoindentation. *J. Mater. Sci.* **2015**, *50*, 7557–7567. [CrossRef]

111. Luo, S.S.; You, Z.S.; Lu, L. Intrinsic fracture toughness of bulk nanostructured Cu with nanoscale deformation twins. *Scr. Mater.* **2017**, *133*, 1–4. [CrossRef]

112. Kim, S.W.; Li, X.Y.; Gao, H.J.; Kumar, S. In situ observations of crack arrest and bridging by nanoscale twins in copper thin films. *Acta Mater.* **2012**, *60*, 2959–2972. [CrossRef]

113. Xiong, L.; You, Z.S.; Qu, S.D.; Lu, L. Fracture behavior of heterogeneous nanostructured 316L austenitic stainless steel with nanotwin bundles. *Acta Mater.* **2018**, *150*, 130–138. [CrossRef]

114. Xiong, L.; You, Z.S.; Lu, L. Fracture behavior of an austenitic stainless steel with nanoscale deformation twins. *Scr. Mater.* **2017**, *127*, 173–177. [CrossRef]

115. Zhu, Y.T.; Liao, X.Z.; Wu, X.L. Deformation twinning in nanocrystalline materials. *Prog. Mater. Sci.* **2012**, *57*, 1–62. [CrossRef]

116. Liu, G.; Zhang, G.J.; Jiang, F.; Ding, X.D.; Sun, Y.J.; Sun, J.; Ma, E. Nanostructured high-strength molybdenum alloys with unprecedented tensile ductility. *Nat. Mater.* **2013**, *12*, 344–350. [CrossRef]

117. Raabe, D.; Ponge, D.; Dmitrieva, O.; Sander, B. Nanoprecipitate-hardened 1.5 GPa steels with unexpected high ductility. *Scr. Mater.* **2009**, *60*, 1141–1144. [CrossRef]

118. Fu, Z.Q.; Jiang, L.; Wardini, J.L.; Macdonald, B.E.; Wen, H.M.; Xiong, W.; Zhang, D.L.; Zhou, Y.Z.; Rupert, T.J.; Chen, W.P.; et al. A high-entropy alloy with hierarchical nanoprecipitates and ultrahigh strength. *Sci. Adv.* **2018**, *4*, 8712. [CrossRef]

119. Wu, X.L.; Yuan, F.P.; Yang, M.X.; Jiang, P.; Zhang, C.X.; Chen, L.; Wei, Y.G.; Ma, E. Nanodomained nickel unite nanocrystal strength with coarse-grain ductility. *Sci. Rep.* **2015**, *5*, 11728. [CrossRef]

120. Yuan, F.P.; Wu, X.L. Size effect and boundary type on the strengthening of nanoscale domains in pure nickel. *Mater. Sci. Eng. A* **2015**, *648*, 243–251. [CrossRef]

121. Ashby, M.F. The deformation of plastically non-homogeneous materials. *Philos. Mag.* **1970**, *21*, 399–424. [CrossRef]

122. Thilly, L.; Van Petegem, S.; Renault, P.-O.; Lecouturier, F.; Vidal, V.; Schmitt, B.; Van Swygenhoven, H. A new criterion for elasto-plastic transition in nanomaterials: Application to size and composite effects on Cu-Nb nanocomposite wires. *Acta Mater.* **2009**, *57*, 3157–3169. [CrossRef]

123. Calcagnotto, M.; Adachi, Y.; Ponge, D.; Raabe, D. Deformation and fracture mechanisms in fine- and ultrafine-grained ferrite/martensite dual-phase steels and the effect of aging. *Acta Mater.* **2011**, *59*, 658–670. [CrossRef]

124. Wang, M.M.; Tasan, C.C.; Ponge, D.; Dippel, A.C.; Raabe, D. Nanolaminate transformation-induced plasticity-twinning-induced plasticity steel with dynamic strain partitioning and enhanced damage resistance. *Acta Mater.* **2015**, *85*, 216–228. [CrossRef]

125. Park, K.; Nishiyama, M.; Nakada, N.; Tsuchiyama, T.; Takaki, S. Effect of the martensite distribution on the strain hardening and ductile fracture behaviors in dual-phase steel. *Mater. Sci. Eng. A* **2014**, *604*, 135–141. [CrossRef]

126. Paul, S.K.; Mukherjee, M. Determination of bulk flow properties of a material from the flow properties of its constituent phases. *Comp. Mater. Sci.* **2014**, *84*, 1–12. [CrossRef]

127. Kelly, A.; Tyson, W.R. Tensile properties of fibre-reinforced metals: copper/tungsten and copper/molybdenum. *J. Mech. Phys. Solids* **1965**, *13*, 329–350. [CrossRef]

128. Ojima, M.; Adachi, Y.; Tomota, Y.; Ikeda, K.; Kamiyama, T.; Katada, Y. Work hardening mechanism in high nitrogen austenitic steel studied by in situ neutron diffraction and in situ electron backscattering diffraction. *Mater. Sci. Eng. A* **2009**, *527*, 16–24. [CrossRef]

129. Chen, B.; Hu, J.N.; Wang, Y.Q.; Zhang, S.Y.; Van Petegem, S.; Cocks, A.C.F.; Smith, D.J.; Flewitt, P.E.J. Role of the misfit stress between grains in the Bauschinger effect for a polycrystalline material. *Acta Mater.* **2015**, *85*, 229–242. [CrossRef]

130. Geng, J.; Nie, J.F. Unloading yield effect in a twin-roll-cast Mg-3Al-1Zn alloy. *Scr. Mater.* **2015**, *100*, 78–81. [CrossRef]

131. Nieh, T.G.; Nix, W.D. Unloading yield effects in aluminum alloys. *Metall. Trans. A* **1986**, *17*, 121–126. [CrossRef]

132. Hart, E.W. Theory of the tensile test. *Acta Metall.* **1967**, *15*, 351–355. [CrossRef]

133. Wang, Y.M.; Ma, E. Three strategies to achieve uniform tensile deformation in a nanostructured metal. *Acta Mater.* **2004**, *52*, 1699–1709. [CrossRef]

134. Zhao, Y.H.; Topping, T.; Bingert, J.F.; Thornton, J.J.; Dangelewicz, A.M.; Li, Y.; Liu, W.; Zhu, Y.T.; Zhou, Y.Z.; Lavernia, E.L. High tensile ductility and strength in bulk nanostructured nickel. *Adv. Mater.* **2008**, *20*, 3028–3033. [CrossRef]

135. Li, Y.S.; Tao, N.R.; Lu, K. Microstructural evolution and nanostructure formation in copper during dynamic plastic deformation at cryogenic temperatures. *Acta Mater.* **2008**, *56*, 230–241. [CrossRef]

136. Fisher, J.C.; Hart, E.W.; Pry, R.H. The hardening of metal crystals by precipitate particles. *Acta Metall.* **1953**, *1*, 336–339. [CrossRef]

137. Eshelby, J.D. The determination of the elastic field of an ellipsoidal inclusion, and related problems. *Proc. R. Soc. Lond. Ser. A* **1957**, *241*, 376–396.

138. Brown, L.M.; Stobbs, W.M. The work-hardening of copper-silica. *Philos. Mag.* **1971**, *23*, 1201–1233. [CrossRef]

139. Atkinson, J.D.; Brown, L.M.; Stobbs, W.M. The work-hardening of copper-silica: IV. The Bauschinger effect and plastic relaxation. *Philos. Mag.* **1974**, *30*, 1247–1280. [CrossRef]

140. Asaro, R.J. Elastic-plastic memory and kinematic-type hardening. *Acta Metall.* **1975**, *23*, 1255–1265. [CrossRef]

141. Monzen, M.; Kawaguchi, Y.; Mori, T. Back stress hardening and static and dynamic softening in a cu alloy with α-Fe particles. *Acta Metall.* **1982**, *30*, 965–972. [CrossRef]

142. Feaugas, X. On the origin of the tensile flow stress in the stainless steel AISI 316L at 300 K: Back stress and effective stress. *Acta Mater.* **1999**, *47*, 3617–3632. [CrossRef]

143. Cottrell, A.H.; Dexter, D.L. Dislocations and Plastic Flow in Crystals. *Am. J. Phys.* **1954**, *22*, 242–243. [CrossRef]

144. Orowan, E. Discussion on internal stresses. In *Symposium on Internal Stresses in Metals and Alloys*; Institute of Metals: London, UK, 1948; pp. 451–453.

145. Orowan, E. Causes and effects of internal stress. *Int. Stress Fat. Met.* **1959**, *7*, 59–80.

146. Moan, G.D.; Embury, J.D. Study of the Bauschinger effect in Al-Cu alloys. *Acta Metall.* **1979**, *27*, 903–914. [CrossRef]

147. Wilson, D.V. Reversible work hardening in alloys of cubic metals. *Acta Metall.* **1965**, *13*, 807–814. [CrossRef]

148. Tomota, Y.; Lukas, P.; Harjo, S.; Park, J.H.; Tsuchida, N.; Neov, D. In situ neutron diffraction study of IF and ultra low carbon steels upon tensile deformation. *Acta Mater.* **2003**, *51*, 819–830. [CrossRef]

149. Xu, Q.; Lavernia, E.J. Influence of nucleation and growth phenomena on microstructural evolution during droplet-based deposition. *Acta Mater.* **2001**, *49*, 3849–3861. [CrossRef]

150. Xu, Q.; Lavernia, E.J. Microstructural evolution during the initial stages of spray atomization and deposition. *Scr. Mater.* **1999**, *41*, 535–540. [CrossRef]

151. Zhang, Y.H.; Zhuang, Y.; Hu, A.; Kai, J.J.; Liu, C.T. The origin of negative stacking fault energies and nanotwin formation in face-centered cubic high entropy alloys. *Scr. Mater.* **2017**, *130*, 96–99. [CrossRef]

152. An, X.H.; Wu, S.D.; Wang, Z.G.; Zhang, Z.F. Significance of stacking fault energy in bulk nanostructured materials: Insights from Cu and its binary alloys as model systems. *Prog. Mater. Sci.* **2019**, *101*, 1–45. [CrossRef]

153. Fischer, F.D.; Reisner, G.; Werner, E.; Tanaka, K.; Cailletaud, G.; Antretter, T. A new view on transformation induced plasticity (TRIP). *Int. J. Plast.* **2000**, *16*, 723–748. [CrossRef]

154. Bouaziz, O.; Guelton, N. Modelling of TWIP effect on work-hardening. *Mater. Sci. Eng. A* **2001**, *319*, 246–249. [CrossRef]

155. Wang, Y.F.; Yang, M.X.; Ma, X.L.; Wang, M.S.; Yin, K.; Huang, A.H.; Huang, C.X. Improved back stress and synergetic strain hardening in coarse-grain/nanostructure laminates. *Mater. Sci. Eng. A* **2018**, *727*, 113–118. [CrossRef]

156. Mughrabi, H. On the current understanding of strain gradient plasticity. *Mater. Sci. Eng. A* **2004**, *387*, 209–213. [CrossRef]

157. Meyers, M.A.; Ashworth, E. A model for the effect of grain size on the yield stress of metals. *Philos. Mag. A* **1982**, *46*, 737–759. [CrossRef]

158. Wang, W.; Yang, M.X.; Yan, D.S.; Jiang, P.; Yuan, F.P.; Wu, X.L. Deformation mechanisms for superplastic behaviors in a dual-phase high specific strength steel with ultrafine grains. *Mater. Sci. Eng. A* **2017**, *702*, 133–141. [CrossRef]

159. Wang, W.; Zhang, H.S.; Yang, M.X.; Jiang, P.; Yuan, F.P.; Wu, X.L. Shock and spall behaviors of a high specific strength steel: Effects of impact stress and microstructure. *J. Appl. Phys.* **2017**, *121*, 135901. [CrossRef]

160. Bouaziz, O.; Allain, S.; Scott, C. Effect of grain and twin boundaries on the hardening mechanisms of twinning-induced plasticity steels. *Scr. Mater.* **2008**, *58*, 484–487. [CrossRef]

161. Wei, Q. Strain rate effects in the ultrafine grain and nanocrystalline regimes-influence on some constitutive responses. *J. Mater. Sci.* **2007**, *42*, 1709–1727. [CrossRef]